IS-T-1847

Hole Burning with Pressure and Electric Field: a Window on the Electronic Structure and Energy Transfer Dynamics of Bacterial Antenna Complexes

by

Wu, Hsing-Mei

PHD Thesis submitted to Iowa State University

Ames Laboratory, U.S. DOE
Iowa State University
Ames, Iowa 50011

Date Transmitted: February 12, 1999

PREPARED FOR THE U.S. DEPARTMENT OF ENERGY
UNDER CONTRACT NO. W-7405-Eng-82.

DISCLAIMER

TABLE OF CONTENTS

* Removed for separate processing —

* Removed for separate processing —

ACKNOWLEDGMENTS

I would like to take this opportunity to express my genuine thanks to those who assisted me during of my graduate research.

I am indebted to my research advisor, Professor Gerald Small, for his guidance, patience and numerous discussions in the past few years. I am fortunate to benefit from his knowledge and insights in various subjects.

Dr. Raja Reddy and Dr. Margus Rätsep deserve my sincere appreciation and much credit for the work presented in this dissertation. I am especially grateful to Dr. Ryszard Jankowiak for his assistance and expertise. I also would like to acknowledge Dr. John Hayes and Dr. Tõnu Reinot for providing their invaluable advice and experience.

I would like to extend my thanks to Kathy Fitzgerald and all the group members, past and present, for the fun and jokes. I am particularly thankful to Nick Milanovich and Kenny Roberts who spent hours proofreading my writing.

My thanks also goes to Derek Brammeier for the laughter we shared during the course of writing this dissertation.

Most of all, I would like to thank my parents and my brother. It was their constant love, support and understanding that kept me focused on completing my graduate studies.

This work was performed at Ames Laboratory under Contract No. W-7405-Eng-82 with the U. S. Department of Energy (DOE). The United States government has assigned the DOE Report number IS-T 1847 to this thesis.

ABSTRACT

Light-harvesting (LH) complexes of cyclic (C_n) symmetry from photosynthetic bacteria are studied using absorption and high pressure- and Stark-hole burning spectroscopies. The B800 absorption band of LH2 is inhomogeneously broadened while the B850 band of LH2 and the B875 band of the LH1 complex exhibit significant homogeneous broadening due to ultra-fast inter-exciton level relaxation. The B800→B850 energy transfer rate of $(\sim 2\ \text{ps})^{-1}$ as determined by hole burning and femtosecond pump-probe spectroscopies, is weakly dependent on pressure and temperature, both of which significantly affect the B800-B850 energy gap. This resilience is theoretically explained in terms of a modified Förster theory with the spectral overlap provided by the B800 fluorescence origin band and weak vibronic absorption bands of B850. Possible explanations for the additional sub-picosecond relaxation channel of B800 observed with excitation on the blue side of B800 are given. Data from pressure and temperature dependent studies show that the B800 and B850 bacteriochlorophyll *a* (BChl *a*) molecules are weakly and strongly excitonically coupled, respectively, which is consistent with the X-ray structure of LH2. The B875 BChl *a* molecules are also strongly coupled. It is concluded that electron-exchange, in addition to electrostatic interactions, is important for understanding the strong coupling of the B850 and B875 rings. The large linear pressure shifts of $\sim -0.6\ \text{cm}^{-1}$/MPa associated with B850 and B875 can serve as important benchmark for electronic structure calculations. The high pressure data obtained for the B800 band, which lead to compressibility values, indicate that the packing of the α, β-polypeptides in the LH2 complex of *Rhodobacter* (*Rb.*) *sphaeroides*, for which a structure is unknown, is looser than for *Rhdopseudomonas* (*Rps.*) *acidophila* whose LH2 structure has been determined. The looser packing is supported by temperature dependent data obtained for the B850 bands. Temperature dependent spectra establish that both the LH2 and LH1 complexes undergo a quite subtle and non-denaturing change near

150 K. Theoretical analysis leads to the conclusion that the nearest neighbor couplings of the B850 and B875 rings are stronger by about 40% for the low temperature structure. Zero-phonon hole action spectroscopy is used to resolve and characterize the lowest energy exciton level (B870) of the B850 ring of A symmetry. The action spectrum indicates that B870 lies 200 cm^{-1} lower in energy than the E_1 level which determines the position of the B850 band maximum. The B870 exciton level, which is forbidden in the absence of energy disorder, carries 3-5% of the total absorption intensity of the B850 ring. A novel theory for analyzing the effects of energy disorder on the exciton level structure of cyclic arrays is presented and used to interpret the experimental results on B870. The theory employs symmetry-adapted basis defect patterns (BDP) which constitute a complete basis set. It is shown that the effects of energy disorder, either diagonal or off-diagonal, on the exciton levels which contribute to the B850 band (including B870) can be largely understood in terms of a single BDP of e_1 symmetry. Relative to "brute force" procedures for analyzing the effects of energy disorder, the new theory simplifies computations and, more importantly, provides far more physical insight. The first Stark hole burning results for photosynthetic complexes are presented. The dipole moment changes ($f \cdot \Delta\mu$) associated with $S_1(Q_y) \leftarrow S_0$ transitions of B800 and B870 of LH2, B896 (the lowest exciton level) of LH1 and B825 of Fenna-Matthews-Olson (FMO) complexes studied fall in the range ~ 0.5-1.2 D. Weak dependencies on laser polarization and burn frequency are observed. That all complexes investigated show linear Stark broadening implies there is a random contribution to $\Delta\mu$ from the "outer shell" of the protein matrix. The presence of Stark splitting, which is only observed in holes burned in B825 of FMO complex, suggests that there is well-defined contribution associated with the "inner shell" of the protein to $\Delta\mu$. Discussion about the consistently larger $f \cdot \Delta\mu$ from classical Stark modulation spectroscopies (it is 3-4 times larger in the case of B850 and B875), as well as the differences between the two Stark techniques, is given. An explanation for the small hole-burning values of $f \cdot \Delta\mu$ for the B870 and B896 levels associated with cyclic arrays of

strongly coupled BChl dimers is given based on structural, symmetry and energy disorder considerations.

CHAPTER 1. INTRODUCTION TO LIGHT-HARVESTING COMPLEXES

1.1 General Introduction to Photosynthesis

The beauty and complexity of photosynthesis go beyond what is indicated by the deceptively simple generalization of CO_2 fixation given by [1, 2]

$$nCO_2 + 2nH_2A + h\nu \rightarrow n(CH_2O) + 2nA + nH_2O. \quad (1.1)$$

Here, A is either oxygen or sulfur. Photosynthesis, which takes place in chloroplasts of higher plants and membranes of prokaryotes, involves delicate interplay between many proteins and pigments; the majority of pigments are either chlorophylls (Chls) or bacteriochlorophylls (BChls). (Figure 1.1 shows the structure of Chl *a* and BChl *a*.) After excitation by light, certain Chls (BChls) are able to initiate charge transfer; electrons are transferred to acceptors and subsequently an electrochemical potential across the photosynthetic membrane is created which drives the reactions which produce energy-rich compounds such as ATP and NADPH.

The classic experiment by Emerson and Arnold in 1932 showed that production of *every* O_2 molecule needed the presence of ~2500 Chls in *Chlorella* cells under saturated illumination [3]. Their observation led to the concept of the *photosynthetic unit* (PSU) in which light is first absorbed by hundreds of Chls or BChls (the *light-harvesting* or *antenna* complexes), as well as other minor pigments such as carotenoids. The excitation energy is then transferred to a specialized non-covalently bounded dimer of Chls (BChls) of the reaction center (RC), the so-called *special pair*, which initiates the electron transfer process after excitation [2, 4, 5]. For purple bacteria, a typical ratio of antenna BChl molecules per special pair ranges from about 100 to 250. That the Chls of RCs lie lower in energy than the light-harvesting (antenna) pigments enables efficient energy funneling to the RC trap. The

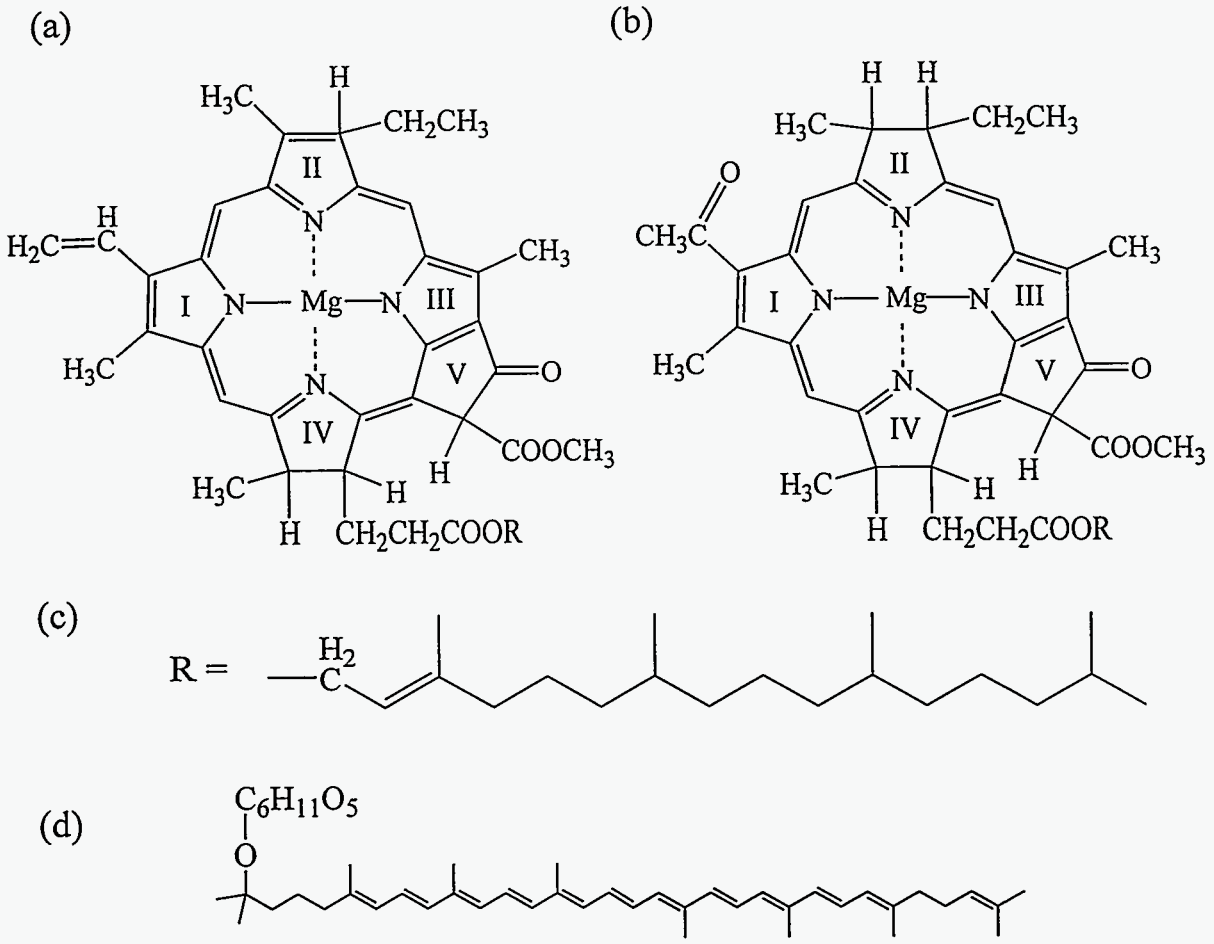

Figure 1.1 Structures of (a) chlorophyll *a*, (b) bacteriochlorophyll *a*, (c) the phytyl chain and (d) rhodopin glucoside. Rhodopin glucoside is the main carotenoid molecules found in light-harvesting complex 2 of purple bacteria *Rhodopseudomonas acidophila*. The phytyl chain is abbreviated as R in structures (a) and (b). The Roman numbers I to V label the rings of Chl and BChl adopted from the IUPAC system. On ring I, Chl *a* has a vinyl group while BChl *a* has acetyl. Furthermore, Chl *a* have one more unsaturated bonds located on ring II than BChl *a*, which contributes to the difference between their absorption band positions. Chl *b* or BChl *b* has one different side chain attached to ring II from Chl *a* or BChl *a*. Pheophytin or bacteriopheophytin molecules are also found in photosynthetic organisms. Their structures are the same as their corresponding Chl or BChl except that the central magnesium is replaced by two protons bonded to rings I and III.

existence of light-harvesting pigments not only broadens the wavelength range of the light absorbed, but also keeps RCs running at an optimal rate. RCs are capable of cycling at a rate of 1000 Hz, while chlorophyll molecules can only absorb photons at a rate ranging from 0.1 Hz in dim light to 10 Hz under direct illumination [5, 6].

1.1.1 Reaction Centers

An important milestone in photosynthesis research in the previous decade was the determination of the high-resolution crystal structure of the RC of the purple bacteria *Rhodopseudomonas viridis* and *Rhodobacter sphaeroides* [7-12] (see Refs. [13, 14] for recent reviews). These structures represent one of the few obtained for membrane proteins which have been solved at atomic resolution. The essential components of the bacterial RC are two protein subunits (L and M) which are approximately related by C_2 symmetry and bind the cofactors. In the bacterial RC, there are the special pair (the primary electron donor), two accessory BChls, two bacteriopheophytin (BPh) molecules and two quinone (Q) molecules which serve as secondary and tertiary electron acceptors, see Figure 1.2. Due to their Q_y absorption band maximum in nanometers, the special pairs of *Rb. sphaeroides* and *Rps. viridis* are named P870 and P960, respectively (P stands for pigments). The former contains BChl *a*, while the latter consists of BChl *b* as the main pigments. The initial electron transfer steps in photosynthesis takes place at very fast rate. The excited P870* transfers an electron to BPh in 3 ps to form $P870^{+}BPh^{-}$. The electron then moves to Q_A, and subsequently to Q_B, in 200 ps and 60 μs, respectively, to further stabilize the charge separation (Q_A and Q_B are the quinone molecules associated with the L and M branches, respectively, see Figure 1.2). $P870^{+}$ becomes active, again, after being reduced by a cytochrome. The same electron transfer process, beginning with excitation of P870, repeats till the fully reduced Q_B^{-2} is formed to combine with protons from cytosol to generate neutral quinol molecules (QH_2). The re-oxidation of QH_2 and electron flow back to P870 via the cytochrome-bc_1 and *c*-type cytochrome complex drive protons outward across the cell membrane, and hence produce

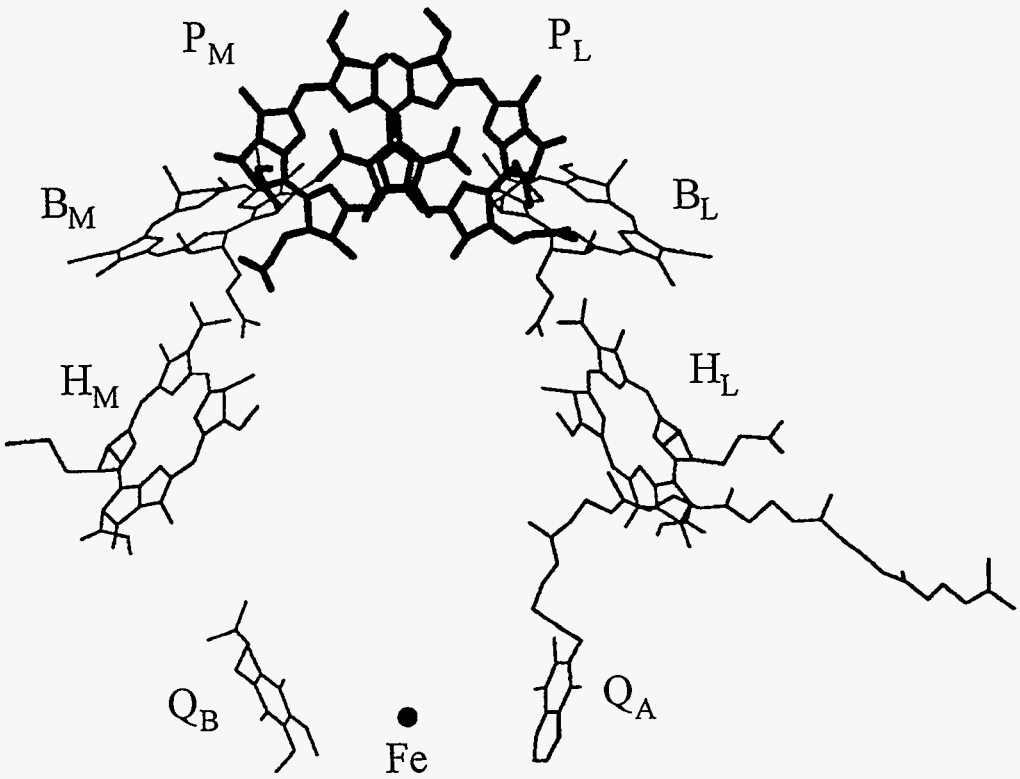

Figure 1.2 Structure of the RC of *Rhodopseudomonas viridis* [7, 8]. P, B, H and Q label the special pair, the accessory BChl, bacteriopheophytin and quinone molecules, respectively. L and M denote the protein branches with which P, B, H are associated. For clarity, the phytyl chains of BChls and bacteriopheophytin molecules are not shown. Q_A and Q_B are the secondary and tertiary electron acceptors, respectively. Fe is a nonheme iron atom present in the reaction center. The figure was generated using the program RasMol [15].

a transmembrane electrochemical potential gradient. ATP synthase utilizes this proton gradient to form ATP. The entire electron flow process is cyclical [16,17]. Though the L and M branches are homologous, the binding and orientations of their associated pigments are slightly different. Electron transfer occurs predominately along the L branch [18]. The aforementioned electron transfer steps also apply to BChl *b* containing P960 from *Rps. viridis*.

In plants and cyanobacteria, there are two types of RC, photosystem II (PS II) and photosystem I (PS I) which work in series (Z scheme, proposed by Hill and Bendall in 1960 [2]), in contrast to only one RC in purple bacteria [2]. Similar to P870 or P960 in bacteria, the primary electron donors of PS I and PS II are referred to as P700 and P680 due to the location in nm of their Q_y absorption bands. Currently, only medium resolution crystal structure (~4.5 Å) of PS I RC is available [19], but protein sequence and other experimental data reveal that PS I and PS II share certain common structural characteristics with RCs of purple bacteria [8, 20]. The strong oxidant produced by excited P680 is used to evolve O_2 from water, while the electron is transferred in several steps to $P700^+$ to re-activate it. The excitation of P700 leads to the formation of NADPH. See, for example, Ref. [21] for more details.

1.2 Light-Harvesting Complexes

As mentioned in the previous section, light-harvesting complexes broaden the range of solar wavelengths used and make the most of the fast RC cycling rate. Recently, advances in obtaining high resolution crystal structure have attracted a lot of research interest in understanding the structure and excitation transfer dynamics of antenna complexes and in developing applications such as artificial antenna and bio-sensors.

To understand the mechanism of the efficient light harvesting and energy transfer processes of antenna complexes, it is essential to know the structures of the protein

complexes, the arrangements and bindings of the pigments in the complexes. The structure provides guidelines for quantum chemical calculations and interpretations of experimental data. Nevertheless, technically speaking it is non-trivial to purify and obtain high-quality, non-denatured 3-D crystals exhibiting good diffraction.

In the mid-1970s, the water-soluble BChl *a* protein from green sulfur bacterium *Prosthecochloris aestuarii* (also known as the FMO complex), which transfers excitation energy from chlorosome to the core antenna of the RC, was shown by X-ray crystallography to contain three protein-pigments subunits arranged with a C_3 symmetry. In each subunit there are seven symmetry-inequivalent BChl *a* [22]. Recently, the structure of the same type of complex from *Chlorobium tepidum* was solved at a resolution of 2.2 Å [23]. It was found that the main structural features of the FMO complex from *Prosthecochloris aestuarii* are conserved. As for plants and green algae, the structure of the isolated Chl *a/b* light-harvesting complex 2 trimers associated with PS II has been determined at a resolution of 3.4 Å, but this level of resolution was not sufficient to allow for differentiation between the Chl *a* and Chl *b* molecules [24].

Of all the photosynthetic protein complexes, antenna and RC complexes of purple non-sulfur bacteria have attracted the most attention due to their overall less congested spectral features. For purple non-sulfur bacteria, there are generally two types of antenna complexes, light-harvesting complexes 1 and 2 (abbreviated as LH1 and LH2). Due to their Q_y absorption maxima in nanometers at room temperature, they are also referred to as B875 and B800-850, respectively. Under different growth conditions, some bacteria, such as *Rhodopseudomonas acidophila*, are capable of having one additional type of antenna, LH3 (B800-820), which absorbs at approximately 800 and 820 nm. Each and every RC is accompanied by one LH1 (B875), while the growth conditions, such as light intensity and temperature, will affect the amount of LH2 per RC. At room temperature, electronic excitation transfer from B800 to B850 occurs in 0.7 ps and is followed by ultra-fast inter-

exciton level relaxation processes within B850 which occur on a ~ 100 fs time scale. B850 → B875 energy transfer occurs in about 3 ps. Following inter-exciton level relaxation within B875, the excitation energy is finally transferred to P870 RC in 50 ps. Figure 1.3 shows the low-temperature absorption spectrum of B800-850 and B875 and a summary of the excitation transfer dynamics. An exciting advance in photosynthesis research was the recently determined X-ray structure of LH2 from *Rps. acidophila* (strain 10050) at 2.5 Å resolution [25, 26]. The structure shown in Figure 1.4 has nine pairs of transmembrane spanning α, β-polypeptides arranged with a C_9 symmetry. Each pair binds two BChl *a* near the periplasmic side which give rise to a Q_y-absorption band at ~ 850 nm, while one BChl *a* bound near the cytoplasmic side absorbs near 800 nm, Figures 1.5 to 1.7. LH2 from another purple bacterium *Rhodospirillum molischianum* was shown to have similar cyclic arrangement [27], except it exhibits C_8 instead of C_9 symmetry.

1.2.1 Crystal Structure of LH2 from *Rps. acidophila* (Strain 10050)

The building block of LH2 is the α, β-polypeptide pairs, Figure 1.5. While the α apoprotein contains 53 amino acids, the β apoprotein consists of 41. Related to each other by C_9 symmetry with the rotational axis perpendicular to the membrane surface, the nine pairs of the polypeptides are arranged in two concentric cylinders with radii of 18 Å for the α and 34 Å for the β apoproteins, Figure 1.4. Both α and β helix axes run nearly parallel to the membrane normal, 2° and 15° respectively. A protomer, the smallest repeating unit of the LH2 structure, is defined as a radially related α, β pair and the associated pigments, which includes three BChl *a* and two carotenoid molecules (rhodopin glucoside, see Figure 1.1(d) for its structure) [25].

The so-called B850 molecules, which are 18 BChl *a* coordinated to histidine residues of the polypeptide pairs (His31 of the α and His30 of the β), form a circle in the space between the α and the β cylinders (Figures 1.5 to 1.7). The molecular planes of those BChl *a* are parallel to the membrane normal and the central magnesium atoms are approximately

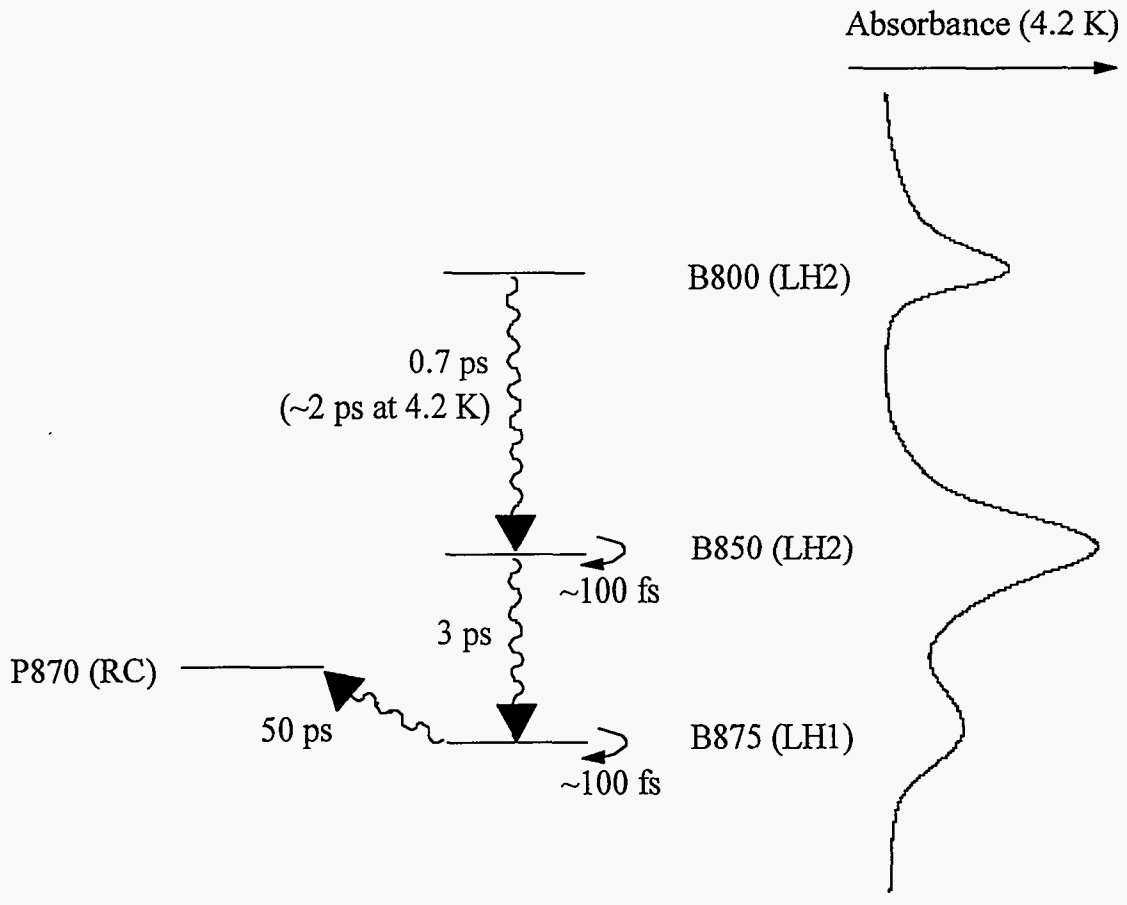

Figure 1.3 Low temperature absorption spectrum of chromatophores of *Rps. acidophila.* At 4.2 K, the B800, B850 and B875 bands are at 12445 cm^{-1} (804 nm), 11495 cm^{-1} (870 nm) and 11055 cm^{-1} (905 nm), respectively. At room temperature, the B850 and B875 bands are not resolved and lead to a single band at 11590 cm^{-1} (863 nm). While the locations of the B850 and B875 bands depend strongly on temperature, the position of B800 is temperature independent. A simple energy level diagram is included on the left to show the transfer times (at room temperature) of different energy transfer steps from B800 to P870 RC. See text.

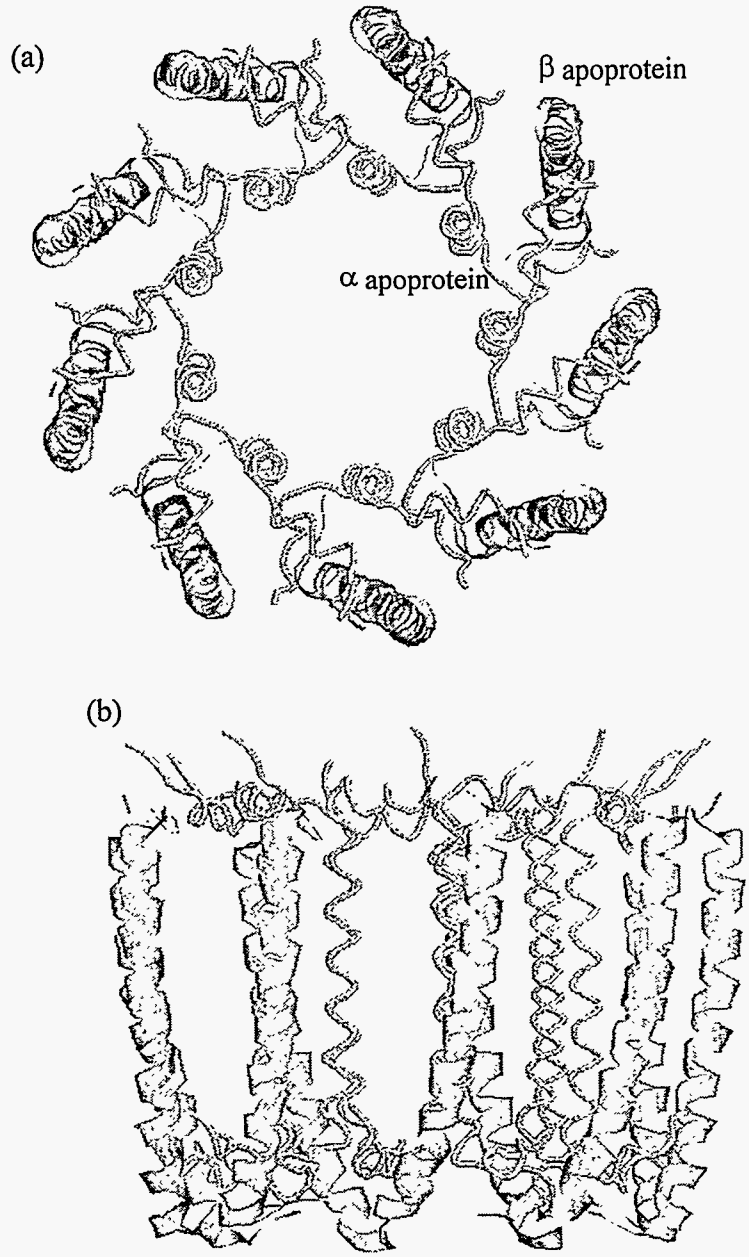

Figure 1.4 The cyclically arranged α, β-polypeptides of the LH2 complex from *Rps. acidophila* (strain 10050) [25, 26]. α polypeptides are on the inner circle with a radius of 18 Å (lighter gray tubes) while β are on the outer circle with a radius of 34 Å (darker gray ribbons). Part (a) shows the view looking down on the membrane from the periplasmic side. Part (b) is a view perpendicular to that of part (a) showing the helices going across the membrane. See text for more details. The figures were generated according to the crystallography coordinates using the RasMol program [15].

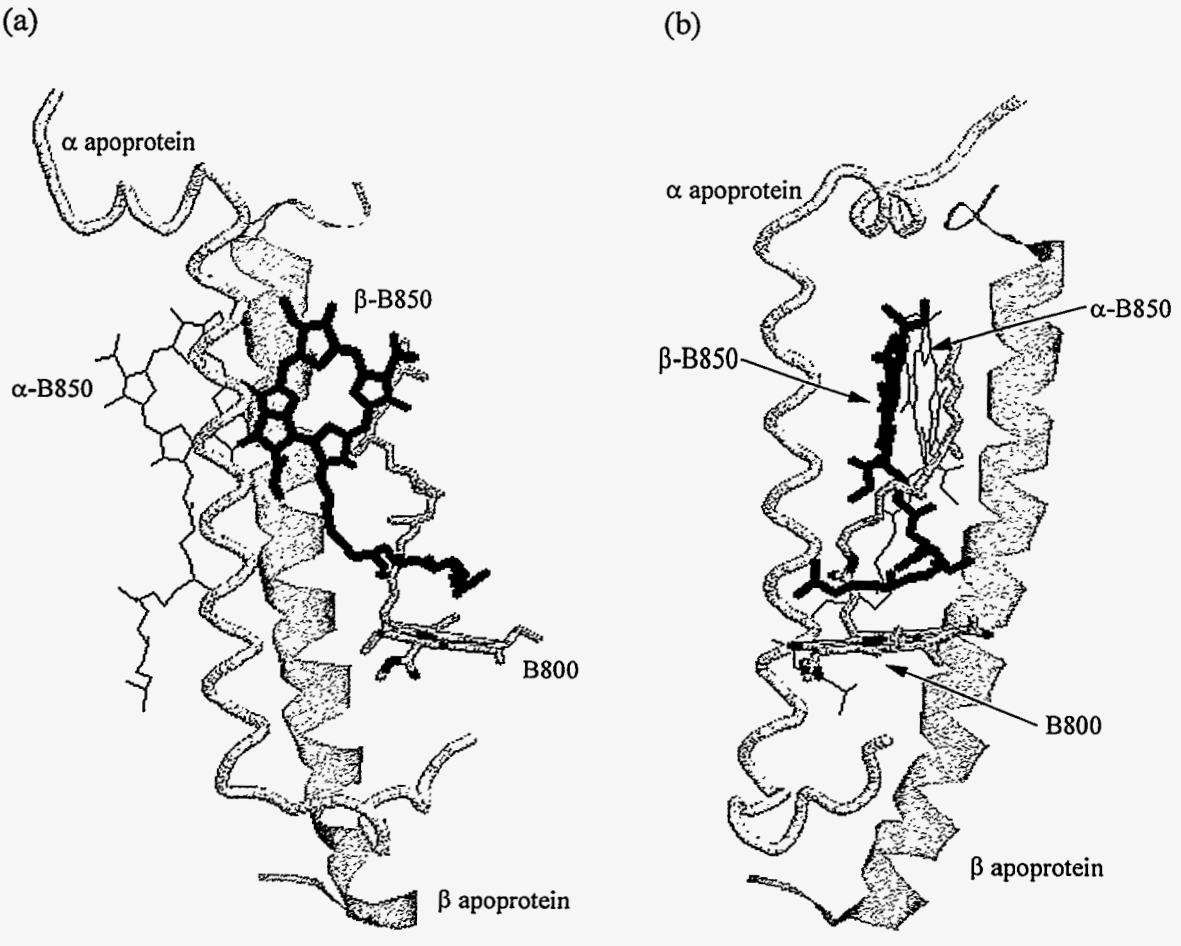

Figure 1.5 Two different views of the protomer (excluding the carotenoid molecules) of the LH2 complex from *Rps. acidophila*, which is the repeating unit of the C_9 complex. As in Figure 1.4, the lighter tube is the α-polypeptide, while the darker gray ribbon is the β-polypeptide. Figure (a) is a view from the C_9 cylinder center. Near the cytoplasmic side (bottom of the figure) is the monomer-like B800 molecule (shown with gray sticks). Near the other side of the membrane, there are two strongly coupled B850 molecules (shown as black wires and sticks respectively). Figure (b) is the side view of (a) with B800 and β-B850 in the foreground and α-B850 in the background. The figures were plotted with RasMol [15].

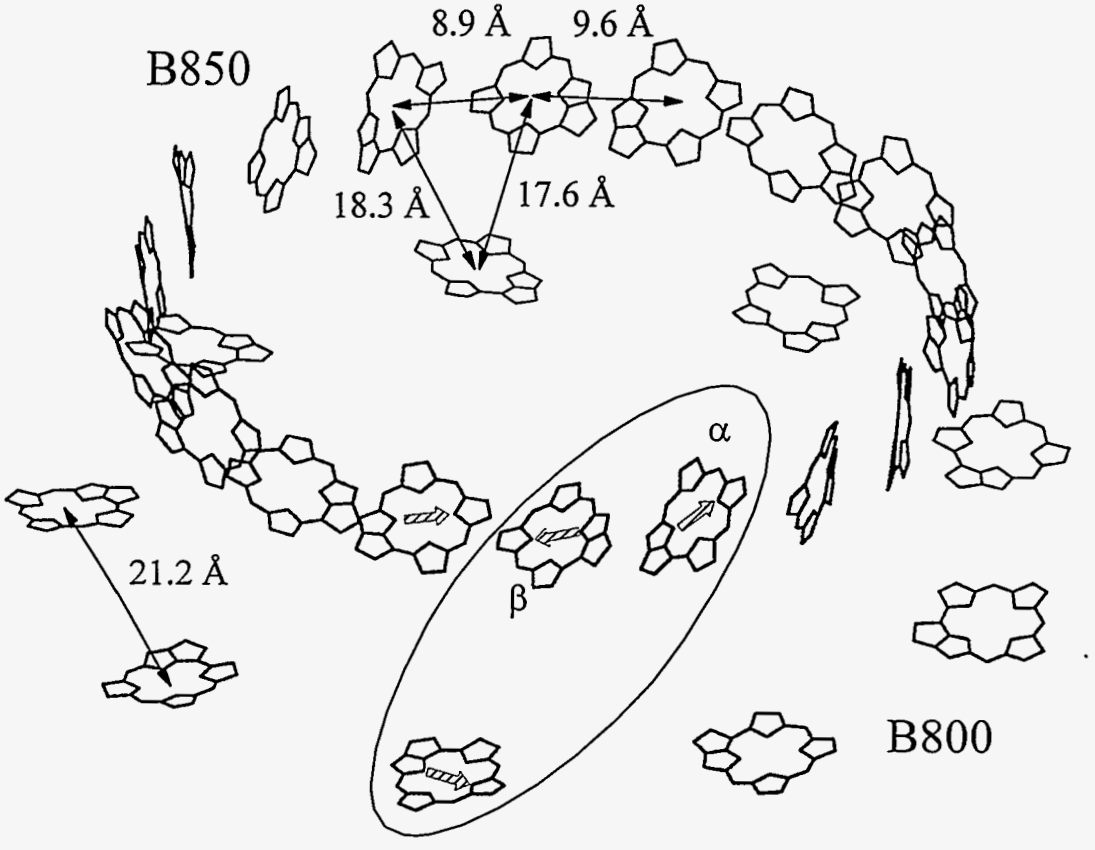

Figure 1.6 Arrangement of the 27 BChls in LH2 of *Rps. acidophila*. The upper ring contains 18 B850 molecules, while the lower ring contains 9 B800 molecules. For clarity, all the side chains on BChls are omitted. The oval encloses the BChls belonging to the same polypeptide pair and the two B850 molecules are labeled by α and β to denote the polypeptides to which they bind. Double-headed arrows mark the Mg...Mg distances between BChls. Note the alternating distances between B850 molecules around the ring. The shaded arrows are drawn to show the directions of Q_y-transition dipole moments of the BChls. See text for more details. This figure was modified from the one made by the RasMol program [15].

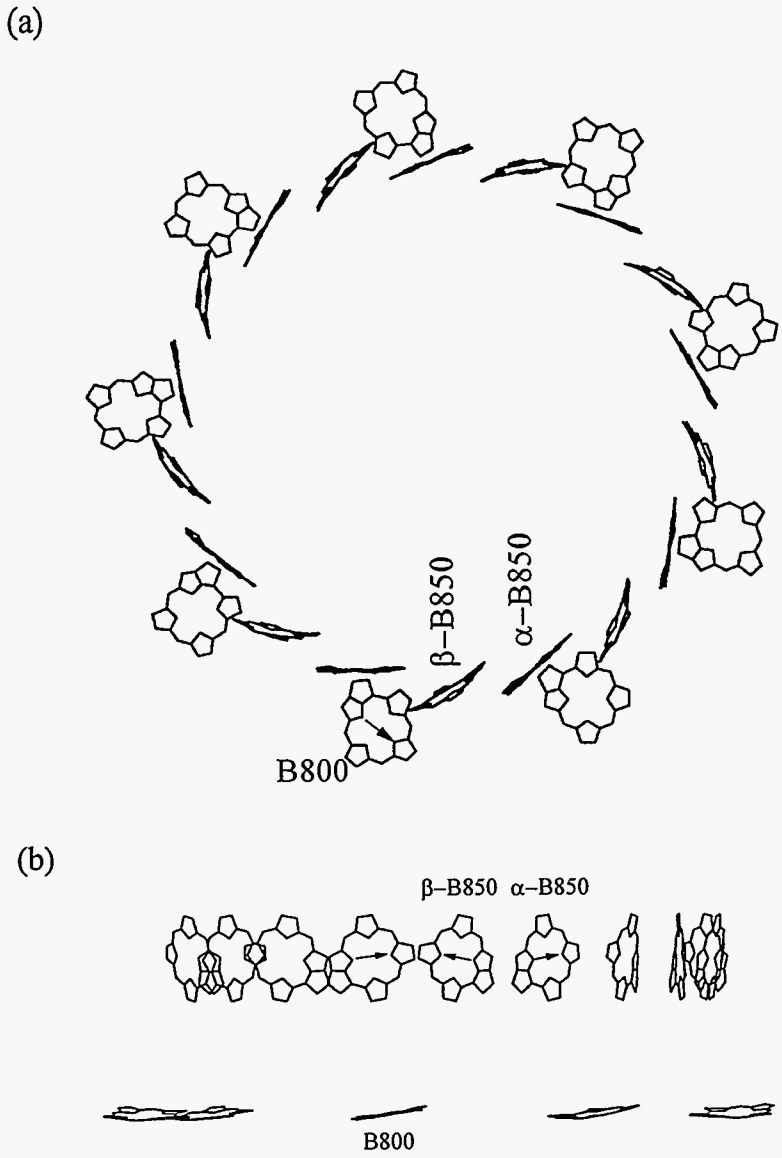

Figure 1.7 (a) Arrangement of the 27 BChl *a* molecules in LH2 of *Rps. acidophila* viewed from the periplasmic side of the membrane. Figure (b) shows the BChls associated with five α, β polypeptide pairs in the lower part of (a) when viewed perpendicular to the C_9 axis. All the side chains on BChls are omitted. In (a) and (b), the arrows show the Q_y-transition dipole moments of B800 and B850 molecules , respectively. The direction of the Q_x-transition dipoles, which is perpendicular to Q_y-transition dipoles by pointing from the nitrogen atom on ring II to that of ring IV, is not shown . For clarity, B800, α-B850 and β-B850 are used to label the three comformationally different BChl *a* molecules associated with one of the polypeptide pairs. The figures were generated by RasMol [15].

10 Å from the presumed periplasmic membrane surface. The Mg…Mg distances for BChl are either 9.6 Å or 8.9 Å with the former being within the protomer, Figure 1.6. Within one protomer, B850 molecules overlap at rings III and V, while between adjacent protomers they overlap at rings I. Due to the C_9 symmetry and the alternating distances, B850 can be viewed as a 9-mer of heterodimers [25, 26, 28-31]. The relative orientation of the transition dipoles of the B850 molecules gives rise to strong Coulombic interactions. The angle between end-to-end Q_y dipoles of B850 within one protomer is 14° and it increases to 26° for neighboring B850 belonging to different protomers (Figures 1.6 and 1.7). The larger angle, however, is compensated by a shorter Mg...Mg distance of 8.9 Å when calculating transition dipole-dipole excitonic coupling which varies inversely as the third power of the distance. Such a short distance of ~ 9 Å and the head-to-head arrangement results in strong Q_y-Q_y coupling interactions (V ~ +300 cm^{-1}) between neighboring BChl molecules [32].

The absorption band at ~ 800 nm is caused by the Q_y-transition of the nine BChl *a* located between β apoproteins, Figures 1.5 to 1.7. Those pigments are held in place by the central magnesium ligated to the carboxyl oxygen of the N-terminal formylmethionine belonging to the α polypeptide [25, 26]. The bacteriochlorin planes are parallel to the cytoplasmic membrane surface which is ~ 11 Å away. As shown in Figures 1.6 and 1.7, the Q_x and Q_y transition dipoles of B800 molecules deviate from the radius and tangent of the nonameric ring by an angle of 15°. The Mg...Mg distance of 21.2 Å makes B800 molecules monomer-like with relatively weak interaction of ~ –25 cm^{-1} as suggested by spectroscopic studies [30, 32-34].

The Mg...Mg distances between B800 and the nearest B850 molecules are either 17.6 Å (with the B850 from the α of the neighboring protomer) or 18.3 Å, see Figure 1.6. The angles of the B800 and the B850 Q_y-transition dipoles corresponding to these two distances are 43° and 105°, respectively. With a separation of ~ 18 Å and the unfavorable

angle, the largest B800-B850 interaction is 27 cm^{-1} [32], which is comparable to the weak B800-B800 coupling mentioned above.

The much stronger couplings between B850 molecules are responsible, in part, for the red shift of the B850 absorption band relative to B800, but there are other factors which contribute to the different band positions [35]. The environment around B800 and B850 molecules is quite different with the former in a relatively polar region and the latter in a hydrophobic region [25]. Besides, B800, α-B850 and β-B850 (the prefixes α- and β- label the polypeptides to which the B850 molecules are bound) distort to different extent and in different ways, which can cause Q_y-energy shift of up to several tens of nanometers [36, 37]. α-B850 molecules show significant hybrid ruffling. Both B800 and β-B850 molecules adopt a standard, slightly bowed conformation with the latter being more planar [26]. In addition, the ligation to Mg^{2+} of B800 molecule is on the opposite face when compared with both types of B850 molecules [35]. There are hydrogen bonds formed between the acetyl oxygen of ring I of all BChls and the polypeptides. B800 has hydrogen bond to the β-Arg20 residue, while the two B850 are hydrogen bonded to α-Trp45 and α-Tyr44, respectively [35].

In addition to BChl *a*, there are also carotenoids which harvest photons in the region from 450 to 570 nm where there is no strong BChl absorption. The most important role played by carotenoids is to serve as the photo-protective agent by quenching the BChl excited triplet state. It is known that this triplet state can readily react with oxygen to produce singlet oxygen whose strong oxidizing power is destructive to the photosynthetic organisms [38, 39].

The carotenoids found in LH2 of *Rps. acidophila* is rhodopin glucoside, see Figure 1.1(d) for its structure. Half of the carotenoid molecules have their glucoside head groups in the hydrophilic pocket in the cytosol region of the membrane, while the others start from the periplasmic side [26]. Their long conjugated hydrocarbon chains extend across the membrane, passing through the B800 and B850 region and making many close contacts with either the phytyl side chains or the main BChl planes, see Figure 1.8. Several contact

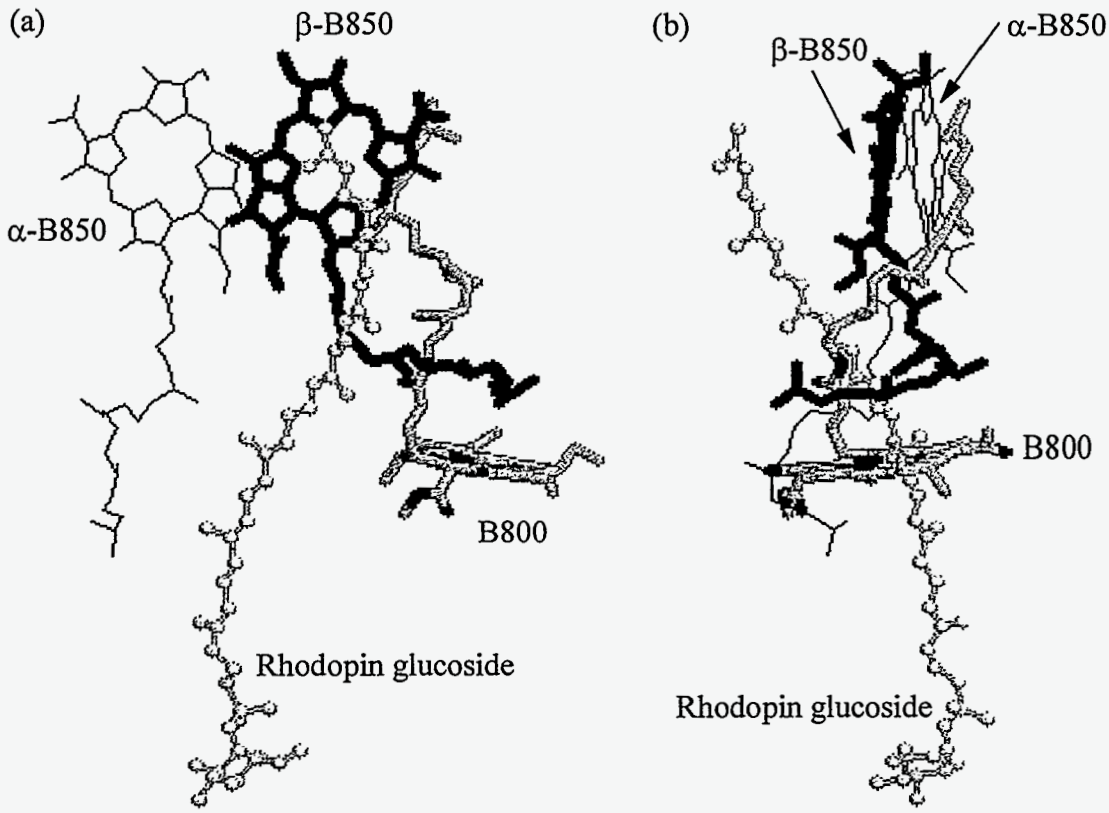

Figure 1.8 The spatial arrangements of rhodopin glucoside, B800 and B850 molecules. The above figures correspond to Figure 1.5(a) and (b), respectively, except that the polypeptide pairs are omitted and the carotenoid molecules are included in Figure 1.8. See text. The other carotenoid revealed in more recent analysis of the crystal structure was not shown in the figure [26]. The images were generated using the program RasMol [15].

distances are as short as ~ 3.5 Å, which may provide for a contribution to B800 → B850 energy transfer from the electron exchange mechanism [26]. As pointed out by Freer *et al.* [26], the presence of carotenoids running across the membrane and making many close contacts with B800 and B850 pigments introduces additional binding stability into the LH2 skeleton.

1.2.2 A Comparison of LH2 Structures from *Rps. acidophila* and *Rs. molischianum*

Shortly after the success of Freer *et al.* [26], a 2.4 Å resolution crystal structure of LH2 from another purple non-sulfur bacterium, *Rs. molischianum,* was determined by molecular replacement using X-ray diffraction [27]. The architectural principles of the two LH2, i.e. the cyclic arrangement of protein pairs and the pigments, are conserved. The major difference is that instead of possessing C_9 symmetry, LH2 from *Rs. molischianum* is a C_8 arrangement of 8 polypeptide pairs [27]. As a result, the B800 and B850 rings of LH2 from *Rs. molischianum* are 8-mer of monomers and heterodimers, respectively. The overall construction of LH2 from *Rs. molischianum* appears to be more tightly packed. The diameters of the inner and outer cylinders formed by the α and β helices are 31 and 62 Å, respectively. The α apoprotein consisting of 27 amino acids deviates from the membrane normal by 2°, while the 34-residue-long β apoprotein is tilted away from the membrane normal by about 10°. As in *Rps. acidophila*, BChl *a* molecules are the major light absorbing pigments. For *Rs. molischianum*, however, lycopene and rhodopin are found to be the major and minor carotenoids, respectively [27, 40]. The B800 BChl molecules sandwiched between β polypeptides are separated from each other by a Mg...Mg distance of 22 Å. The Mg...Mg distances between nearest neighbor B850 molecules are 9.2 Å within the protomer and 8.9 Å between nearest protomers, as compared with 9.6 and 8.9 Å in *Rps. acidophila.* The Mg...Mg distances between B800 and the nearest B850 molecules are either 19.1 Å (with the B850 from the α of the neighboring protomer) or 20.2 Å. The angles between the Q_y-transition dipole moments of B800 and the nearest B850 molecules are 13.1° and 151.5°,

respectively. The longer B800-B850 distances observed in LH2 of *Rs. molischianum* are less favored for Förster energy transfer than *Rps. acidophila* , but are compensated by larger κ^2 values, see Eqs. (2.3) and (2.4).

The most apparent difference between these two LH2 complexes is associated with B800 binding and orientation. B800 molecules of *Rs. molischianum* are bound to an aspartate residues of the α-apoprotein, instead of formylmethionine residues as observed for *Rps. acidophila*. For LH2 of *Rs. molischianum*, the B800 macrocycles deviate from the membrane surface by 38° (though the Q_y-transition dipole moments are parallel to the membrane plane to within 10°), which is nearly twice the angle (18°) observed in *Rps. acidophila*. From the superposition of the α, β pairs from these two LH2 [27], a roughly 90° rotation has to be applied in order to overlap the projection of Q_y-transition dipoles on the membrane. Consequently, for *Rs. molischianum* and *Rps. acidophila*, the Q_y-transition dipole of the B800 molecule is approximately parallel and perpendicular to that of the α-B850 molecule in the same protomer, respectively.

Although the binding and the orientation of B800 molecules in *Rs. molischianum* and *Rps. acidophila* are quite different, the absorption properties and B800 → B850 energy transfer time are very similar, see Refs. [30, 41].

1.2.3 Projection Structure of LH1 Complex from *Rhodospirillum rubrum*

In 1995, Karrasch *et al.* reported a projection map of the LH1 (B875) complex of purple non-sulfur bacterium *Rhodospirillum rubrum* at a resolution of 8.5 Å [42]. LH1 is the only antenna complex of *Rs. rubrum*. The data indicate that the cyclic arrangements seen in LH2 exist in LH1 but LH1 possesses a larger ring size than LH2. The building block is an α, β-polypeptide pairs with 52 (α) and 54 (β) amino acid residues. 16 polypeptide pairs aggregate to form a C_{16}-ring with an outer diameter of 116 Å and an inner diameter of 68 Å, which is large enough to house RC within. LH1 complex exhibits a single Q_y-absorption band at 880 nm which exhibits significantly homogeneous broadening due to inter-exciton

level relaxation processes [42]. The locations of pigments in the complex are not clearly resolved due to the limited resolution of 8.5 Å. Based on the LH2 structure, the conserved histidine residues and spectroscopic properties , the BChls which contribute to the 880-nm band are believed to lie edge-on between α and β polypeptides as in the case of the B850 molecules of LH2. The density observed in the projection map suggests that B875 BChls are strongly interacting with neighboring B875 with an estimated nearest Mg...Mg separation of ~ 7.5 Å [42], which is also similar to B850 molecules.

1.2.4 Organization of Photosynthetic Complexes in the Membrane of Purple Bacteria

It is generally accepted that RC is located inside the LH1 ring. However, the exact arrangement of the LH2 complexes around the LH1-RC unit in the natural membrane is unknown. Several models have been proposed. For example, Monger and Parson proposed a clustered model with an aggregate of several LH1-RC surrounded by LH2 [43]. Recently, Papiz *et al.* suggested a building unit of one LH1-RC enclosed by eight cyclically arranged LH2 complexes [44]. They argued that their model has the flexibility of accommodating other membrane proteins and it can give an ordered and hexagonally-packed units of sixfold symmetry in accordance with the low resolution electron microscopic data [45]. See Ref. [44] for further discussion.

Recently, Hu and Schulten [46] employed molecular dynamics simulations and energy minimization to model the structure of LH1 of *Rb. sphaeroides* with its RC located inside the ring. Taking advantage of the high degree of homology of the α, β-polypeptide pairs of LH1 of *Rb. sphaeroides* to those of LH2 of *Rs. molischianum*, the structure of the former complex is modeled as a 16-mer by using the C_8 arrangement of the latter as a template. The conserved histidine residues, α-His32 and β-His39, are the binding sites for B875 BChl *a* molecules. The shortest Mg...Mg distance between B875 BChl *a* molecules and the RC special pair (P_L or P_M) is 42 Å, while it is 35 Å between the B875 and accessory BChl molecules. The planes of tryptophan residues in the LH1-RC complex and the LH2

complex are used to align the pigment-protein complexes of the basic PSU, which is one LH2 complex in contact with one LH1-RC unit. The B850 BChls of LH2 and the B875 BChls of LH1 are exactly coplanar, which is the optimal arrangement for excitation energy transfer to the RC. See Ref. [46] for more details.

1.3 Application of Hole Burning Spectroscopy to Light-Harvesting Complexes

This dissertation presents the results of the candidate's original studies on light-harvesting complexes by high pressure- and Stark-hole burning as well as theoretical results on the effects of energy disorder using symmetry-adapted basis defect patterns.

1.3.1 Marriages of Non-Photochemical Hole Burning Spectroscopies with High Pressure and Electric Field

After the pioneering works of Kharlamov, Personov, and Bykovskaya [47] and Gorokhovskii, Kaarli and Rebane [48] in 1974, persistent spectral hole burning in crystalline and amorphous solids has proven to be one of the most powerful frequency-domain spectroscopies. Excellent general reviews on hole burning may be found in Refs. [49-51]. Later, non-photochemical hole burning proved to be an unrivaled frequency-domain tool for the study of photosynthetic protein complexes since it provides information on Q_y-electronic structure, structural heterogeneity and inhomogeneous spectral broadening, distributions of donor-acceptor energy gap values, electron-protein phonon coupling, Chl (BChl) vibrational frequencies/Franck-Condon factors and transport dynamics from zero-point level. See Refs. [52, 53] and references listed in Ref. [51].

Following the success of Small and coworkers [54, 55] in applying hole burning with high pressure to study photosynthetic reaction centers and the FMO complex, the same combination is further employed to investigate antenna complexes from purple bacteria, which is the main focus of the candidate's work. The beauty of the high pressure experiment is the ability to continuously tune spectroscopic properties via the pressure-induced changes

in relative orientations of pigments and their separation as well as changes in pigment-protein distances. In a sense, a new "*mutant*" of the complex is obtained at every pressure. Thus, a much more systematic approach to understanding electronic structure and transport dynamics becomes available.

Recently, Stark hole burning was performed successfully for the first time on photosynthetic antenna complexes [56, 57]. Information such as the dipole moment changes associated with the transitions from the ground to excited states and charge transfer interactions can be extracted from the data. Due to the narrowness of zero-phonon holes, only moderate electric field strength is required for Stark hole burning as compared with the classical Stark modulation experiment performed on the whole absorption band.

Hole burning, high pressure, and Stark experimental setups are given in Refs. [58], [54] and [57], respectively, as well as in the related chapters of this dissertation.

1.4 Thesis Organization

Chapter 1 gives a general background on photosynthesis and light-harvesting complexes. The emphasis is placed on the description of high resolution crystal structures of antenna complexes from purple bacteria. Chapter 2 is a short review on mechanisms of excitation energy transfer and relaxation including theories of Förster energy transfer, electron exchange and molecular excitons. Chapter 3 to 7 are selections of published or accepted papers of the candidate. In Chapter 3, high-pressure hole burning and femtosecond pump-probe spectroscopies are used to study B800→B850 energy transfer kinetics of LH2 complex from *Rps. acidophila* (strain 10050). Comparisons of LH2 from *Rps. acidophila* and *Rb. sphaeroides* are given in Chapter 4 using different combinations of absorption or hole burning spectroscopies with temperature or pressure. The studies related to the effects of energy disorder on the B850 exciton level structure and spectroscopic properties are contained in Chapters 5 and 6. The former is aimed towards understanding B850's exciton

level structure by using symmetry-adapted basis defect patterns to account for the experimentally observed oscillator strength and energy splittings of the exciton levels. The latter deals with the effects of energy disorder on exciton level localization and the implications of localization on the interpretation of Stark hole burning data. Chapter 7 describes and discusses the Stark hole burning results obtained for three types of antenna complexes from photosynthetic bacteria. The shortcomings of classical Stark modulation spectroscopies are also discussed in Chapter 7. General conclusions are given in Chapter 8. The appendix provides detailed derivations of the theoretical equation used in Chapters 5 and 6.

1.5 Other Published Work of the Candidate

The following are titles of papers not included in this dissertation in chronological order:

- High Pressure Studies of Excitonically Coupled Photosynthetic Antenna Complexes [59].
- Pressure Dependence of Energy and Electron Transfer in Photosynthetic Complexes [60].
- High Pressure Studies of Energy Transfer and Strongly Coupled Bacteriochlorophyll Dimers in Photosynthetic Protein Complexes [34].
- A Comparison of the LH2 Antenna Complex of Three Purple Bacteria by Hole Burning and Absorption Spectroscopies [41].
- Direct Observation and Hole Burning of the Lowest Exciton Level (B870) of the LH2 Antenna Complex of *Rhodopseudomonas acidophila* (Strain 10050) [28].
- Symmetry Adapted Basis Defect Patterns for Analysis of the Effects of Energy Disorder on Cyclic Arrays of Coupled Chromophores [29].
- Stark Hole Burning Spectroscopy of a Photosynthetic Complex: LH2 of Purple Bacteria [56].

- Hole Burning and Absorption Studies of the LH1 Antenna Complex of Purple Bacteria: Effects of Pressure and Temperature [61].

1.6 References

[1] Stryer, L. *Biochemistry,* 3rd Ed.; Freeman and Company: New York, 1988; Chapter 22.

[2] Zubay, G. *Biochemistry,* 3rd Ed.; Wm. C. Brown Publishers: Dubuque, 1993; Chapter 16.

[3] Emerson, R.; Arnold, W. *J. Gen. Physiol.* **1932**, *16*, 191.

[4] Duysens, L. N. M. *Transfer of Excitation Energy in Photosynthesis*, Ph. D. Thesis, State University of Utrecht, 1952.

[5] Mauzerall, D.; Greenbaum, N. L. *Biochim. Biophys. Acta*, **1989**, *974*, 119.

[6] van Grondelle, R.; Sundström, V. In *Photosynthetic Light-Harvesting Systems*, Scheer, H. Ed.; Walter de Gruyter & Co.: Berlin, New York, 1988: p 403.

[7] Deisenhofer, J.; Epp. O.; Miki, K.; Huber, R.; Michel, H. *J. Mol. Biol.* **1984**, *180*, 385.

[8] Deisenhofer, J.; Epp. O.; Miki, K.; Huber, R.; Michel, H. *Nature*, **1985**, *318*, 618.

[9] Allen, J. P.; Feher, G.; Yeates, T. O.; Rees, D. C.; Deisenhofer, J.; Michel. H.; Huber, R. *Proc. Natl. Acad. Sci. U. S. A.* **1986**, *83*, 8593.

[10] Arnoux, B.; Decruis, A. Reiss-Husson, F.; Lutz, M.; Norris, J.; Schiffer, M.; Chang, C. H. *FEBS Lett.* **1989**, *258*, 47.

[11] El-Kabbana, O.; Chang, C. H.; Tiede, D.; Norris, J.; Schiffer, M. *Biochem.* **1991**, *30*, 5361.

[12] Deisenhofer, J. Epp. O.; Sinning, I; Michel, H. *J. Mol. Biol.* **1995**, *246*, 429.

[13] Lancaster, C. R. D.; Ermler, U.; Michel, H. In *Anoxygenic Photosynthetic Bacteria*, Blankenship. R. E.; Madigan, M. T.; Bauer, C. E. Ed.; Kluwer Academic Publishers: Dordrecht, 1995: Chapter 23.

[14] Deisenhofer, J.; Michel, H. In *Chlorophylls*, Sheer, H. Ed.; CRC Press: Boca Raton, 1991, p. 617.

[15] Sayle, R.; Milner-White, E. J. *Trends Biochem. Sci.* **1995**, *20*, 374.

[16] Pierson, B. K. *Arch. Microbiol.* **1985**, *143*, 260.

[17] Zannoni, D.; Ingledew, W. J. *Febs. Lett.* **1985**, *193*, 93.

[18] Michel-Beyerle, M. E.; Plato, M.; Deisenhofer, J.; Michel, H.; Bixon, M.; Jortner, J. *Biochim. Biophys. Acta*, **1988**, *932*, 52.

[19] Fromme, P.; Witt, H. T.; Schubert, W.-D.; Klukas, O.; Saenger, W.; Krauss, N. *Biochim. Biophys. Acta* **1996**, *1275*, 76.

[20] Rochaix, J. D.; Dron, M.; Rahire, M.; Malnoe, P. *Plant Mol. Biol.* **1984**, *3*, 363.

[21] Mathis, P.; Rutherford, A. W. *New Comprehensive. Biochem.* **1987**, *15*, 63.

[22] Tronrud, D. E.; Schmid, M. F.; Matthews, B. W. *J. Mol. Biol.* **1986**, *188*, 443.

[23] Li, Y.-F.; Zhou, W.; Blankenship, R. E.; Allen, J. P. *J. Mol. Biol.* **1997**, *271*, 456.

[24] Kühlbrandt, W.; Wang, D. N. Fujiyoshi, Y. *Nature*, **1994**, *367*, 614.

[25] McDermott, G.; Prince, S. M.; Freer, A. A.; Hawthornthwaite-Lawless, A. M.; Papiz, M. Z.; Cogdell, R. J.; Isaacs, N. W. *Nature* **1995**, *374*, 517.

[26] Freer, A.; Prince, S; Sauer, K.; Papiz, M.; Hawthornthwaite-Lawless, A.; McDermott, G.; Cogdell, R.; Isaacs, N. W. *Structure* **1996**, *4*, 449.

[27] Koepke, J.; Hu, X.; Muenke, C.; Schulten, K. Michel, H. *Structure*, **1996**, *4*, 581.

[28] Wu, H.-M.; Reddy, N. R. S.; Small, G. J. *J. Phys. Chem. B* **1997**, *101*, 651.

[29] Wu, H.-M.; Small, G. J. *Chem. Phys.* **1997**, *218*, 225.

[30] Chapter 4; Wu, H.-M.; Ratsep, M.; Jankowiak, R.; Cogdell, R. J.; Small, G. J. *J. Phys. Chem. B* **1997**, *101*, 7641.

[31] Chapter 5; Wu, H.-M.; Ratsep, M.; Lee, I.-J.; Cogdell, R. J.; Small, G. J. *J. Phys. Chem. B* **1997**, *101*, 7654.

[32] Sauer, K.; Cogdell, R. J.; Prince, S. M.; Freer, A. A.; Isaacs, N. W.; Scheer, H. *Photochem. Photobiol.*, **1996**, *64*, 564.

[33] Cogdell, R. J.; Scheer, H. *Photochem. Photobio.* **1985**, *42*, 669.

[34] Reddy, N. R. S.; Wu, H.-M.; Jankowiak, R.; Picorel, R.; Cogdell, R. J.; Small, G. J. *Photosynth. Res.* **1996**, *48*, 277.

[35] Prince, S. M.; Papiz, M. Z.; Freer, A. A.; McDermott, G.; Hawthornwaite-Lawless, A. M.; Cogdell, R. J.; Isaacs, N. W. *J. Mol. Biol.* **1997**, *268*, 412.

[36] Gudowska-Nowak, E.; Newton, M. D.; Fajer, J. *J. Phys. Chem.* **1990,** *94*, 5795.

[37] Gentemann, S.; Nelson, N. Y.; Jaquinod, L.; Nurco, D. J.; Leung, S. H.; Medforth, C. J.; Smith, K. M.; Fajer, J.; Holten, D. *J. Phys. Chem. B* **1997**, *101*, 1247.

[38] Sietermann, D. *Biochim. Biophys. Acta* **1985**, *811*, 325.

[39] Cogdell, R. J.; Frank, H. A. *Biochim. Biophys. Acta* **1987**, *895*, 63.

[40] Germeroth, L; Lottspeich, F.; Robert, B.; Michel, H. *Biochem.* **1993**, *32*, 5615.

[41] Wu, H.-M.; Reddy, N. R. S.; Cogdell, R. J.; Muenke, C.; Michel, H.; Small, G. J. *Mol. Cryst. Liq. Cryst.* **1996**, *291*, 163.

[42] Karrasch, S.; Bullough, P. A.; Ghosh, R. *EMBO J.* **1995**, *14*, 631.

[43] Monger, T. G.; Parson, W. P. *Biochim. Biophys. Acta* **1977**, *460*, 393.

[44] Papiz, M. Z.; Prince, S. M.; Hawthornthwaite-Lawless, A. M.; McDermott, G.; Freer, A. A.; Isaacs, N. W.; Cogdell, R. J. *Trends in Plant Sci.* **1996**, *1*, 198.

[45] Miller, K. R. *Nature* **1982**, *300*, 53.

[46] Hu, X.; Schulten, K. *Biophys. J.* submitted.

[47] Kharlamov, B. M.; Personov, R. I.; Bykovskaya, L. A. *Opt. Commun.* **1974**, *12*, 191.

[48] Gorokhovskii, A. A.; Kaarli, R. K.; Rebane, L. A. *JETP Lett.* **1974**, *20*, 216.

[49] Moerner, W. E. Ed. *Persistent Spectral Hole Burning: Science and Applications*; Springer-Verlag: Berlin, 1988.

[50] Völker, S. In *Relaxation Processes in Molecular Excited States*, Fünfschilling, J. Ed.; Kluwer: Dordrecht, 1989; p. 113.

[51] Jankowiak, R.; Hayes, J. M.; Small, G. J. *Chem. Rev.* **1993**, *93*, 1471.

[52] Köhler, W.; Friedrich, J.; Fischer, R.; Scheer, H. *J. Chem. Phys.* **1988**, *89*, 871.

[53] van der Laan, H.; Schmidt, Th.; Visschers, R. W.; Visscher, K. J.; van Grondelle, R.; Völker, S. *Chem. Phys. Lett.* **1990**, *170*, 231.

[54] Reddy, N. R. S.; Jankowiak, R.; Small, G. J. *J. Phys. Chem.* **1995**, *99*, 16168.

[55] Chang, H.-C.; Jankowiak, R.; Reddy, N. R. S.; Small, G. J. *Chem. Phys.* **1995**, *197*, 307.

[56] Rätsep, M.; Wu, H.-M.; Hayes, J. M.; Small, G. J. *Spectrochim Acta A*, in press.

[57] Chapter 7; Rätsep, M.; Wu, H.-M.; Hayes, J. M.; Blankenship, R. E.; Cogdell, R. J.; Small, G. J. *J. Phys. Chem. B* **1998**, in press.

[58] Lyle, P. A.; Kolaczkowski, S. V.; Small, G. J. *J. Phys. Chem.* **1993**, *97*, 6924.

[59] Reddy, N. R. S.; Wu, H.-M.; Jankowiak, R.; Small, G. J. In *High Pressure Science and Technology, Proceedings of the Joint XV AIRAPT & XXXIII EHPRG International Conference*, Trzeciakowski, W. Ed.; Warsaw, Poland, 1996, p 878.

[60] Reddy, N. R. S.; Chang, H.-C.; Wu, H.-M.; Jankowiak, R.; Small, G. J. In *Proceedings of Third Feldafing International Workshop on Reaction Center of Photosynthetic Bacteria: Structure and Dynamics*, M. E. Michel-Beyerle, Ed.; Springer-Verlag, 1996, p 255.

[61] Wu, H.-M.; Rätsep, M.; Jankowiak, R.; Cogdell, R. J.; Small, G. J. *J. Phys. Chem. B*, **1998**, in press.

CHAPTER 2. MECHANISMS FOR EXCITATION ENERGY TRANSFER AND RELAXATION

2.1 Introduction

Understanding electronic excitation energy transfer in photosynthetic antenna complexes is of very considerable importance. It is the process which precedes primary charge separation process in RC. Energy transfer is often treated in two limits, strong and weak coupling between the donor (D) and acceptor (A) molecules (states). An important criterion for weak coupling is that the interaction between D and A is small relative to their electronic energy gap. When this gap is small, the homogeneous broadenings of the D and A levels due to dephasing must be small relative to the D-A energy gap. The Förster theory of electronic energy transfer [1, 2] is a weak coupling theory developed to understand energy transfer between donor and acceptor molecules in liquids. The interaction between D and A was taken to be of the transition dipole-dipole type. Later, Dexter extended the theory to include exchange coupling involving two-electron exchange integrals and higher multipole interactions [3]. Nevertheless, the Förster-Dexter theory is a weak coupling theory whose energy transfer rate expression stems from the Fermi-Golden rate expression with the "trigger" being the static intermolecular potential energy. Furthermore, the theory was not designed for solids such as photosynthetic complexes whose optical absorption and fluorescence transitions suffer from significant inhomogeneous broadening, *vide infra*.

Förster-Dexter theory, which has been widely applied in photosynthesis, is inapplicable when one is confronted with an array of strongly coupled and identical (chemically) Chl molecules [4, 5]. Strong coupling means that the nearest neighbor Chl-Chl interactions are much larger than the homogeneous width of the Chl optical transition. Strong coupling, with static lattice approximation, means that the Hamiltonian which determines the excitonic wavefunctions and energies already includes the static

intermolecular potential energy. Thus, relaxation between exciton levels is induced by phonons which modulate the intermolecular pigment-pigment interactions. The B850 and B875 rings of BChl molecules are prime candidates for such a situation, although the effects of energy disorder from structural heterogeneity must be taken into account. That is, if the disorder-induced splittings between the exciton levels are much larger than the nearest neighbor coupling, the exciton levels will no longer be delocalized on individual molecules. In this case, weak coupling energy transfer theory would become applicable and energy transfer thought of as an incoherent hopping process [6].

As discussed in Chapter 3, the interactions between the B800 and B850 molecules of the LH2 complex are weak enough for B800 → B850 transfer to be describable by a modified Förster theory which takes into account structural heterogeneity, *vide infra.*

2.1.1 Energy Transfer in Photosynthesis

Energy transfer consistent with the Förster mechanism has been observed in various types of donor-acceptor systems in solutions or solids. Of particular relevance to this dissertation is the mechanism for B800 → B850 transfer in the LH2 complex which has been extensively studied by ultrafast pump-probe and hole burning spectroscopies [7-13]. The LH2 structure which yields a nearest neighbor B800-B850 distance of 17.6 Å and a dipole-dipole orientation factor κ of 0.78 [14] results in a weak coupling of 27 cm^{-1} [15]. This favors Förster-type energy transfer. The Dexter-type electron exchange mechanism for B800 → B850 transfer is unimportant because of the large separation distances. However, it provides the route for both the deactivation of triplet BChl, which is harmful to the bacteria, by a triplet carotenoid state [16, 17] as well as symmetry-forbidden singlet-singlet energy transfer from the 2^1A_g state of carotenoid to the BChl *a* Q_y state [2, 18-20]. The nearly co-linear arrangement of adjacent B850 Q_y-transition dipoles (κ =1.67 and 1.19) and the short nearest neighbor B850-B850 separation distance (~ 9 Å) gives rise to a strong excitonic interaction, ~ 300 cm^{-1} according to Sauer *et al.* [15]. Hole-burning studies have indicated a

fast relaxation among exciton levels (~ 100 fs) and have been used to characterized the spectroscopic properties of the lowest exciton level of strongly-coupled B850 BChl *a* molecules [11, 21-24].

The three types of energy transfer mechanisms mentioned above are discussed separately in the remaining part of this chapter. In addition, a modified Förster theory for energy transfer developed by Small and coworkers [25] which is based on the Fermi-Golden rule is also presented. This theory has been successfully applied to explain the resilience of B800 → B850 energy transfer rates to pressure and temperature [13, 26] as well as to species and mutations which changes the B800-B850 energy gap by several hundred wavenumbers [27, 28].

2.2 Förster Energy Transfer

2.2.1 Conventional Förster Theory

Förster transfer between the excited state, D*, of donor molecules and acceptor molecules (A) in dilute solids or liquids where the average D-A separation distance is $\gtrsim$ 20 Å has been thoroughly studied [1]. (The trivial mechanism of reabsorption by A of the photon emitted by D* is easily distinguished from Förster transfer since it does not lead to a shortening of D*'s lifetime [29].)

In the limit of weak coupling between D and A molecules, the transition rate from the initial state $|D^*A\rangle$ to the final state $|DA^*\rangle$ is given by the Fermi-Golden rule [30]:

$$k_{ET} = \frac{2\pi}{\hbar}\left|\langle D^*A|V|DA^*\rangle\right|^2 \rho(E), \tag{2.1}$$

where V is the molecular interaction between D and A and $\rho(E)$ is the density of final states isoenergetic with the initial D* levels. $\rho(E)$ is referred to as the Franck-Condon factor weighted density of states associated with vibrations when the Condon approximation is employed, which is an excellent approximation for strongly allowed electronic transitions.

Strictly speaking, $\rho(E)$ depends on temperature. Förster theory assumes that thermalization of the molecular vibrations and bath phonons occurs on a faster time scale than energy transfer. V can be expressed by a multipole expansion [2, 31]. In Förster theory, the dipole-dipole approximation is employed so that the matrix element in Eq. (2.1) is

$$V_{dd} = \kappa|\vec{\mu}_D||\vec{\mu}_A|/R^3, \tag{2.2}$$

where $R \equiv |\vec{\mathbf{R}}_{DA}|$ is the distance from the center of molecule D to that of molecule A and $\vec{\mu}_D$ and $\vec{\mu}_A$ are the electronic transition dipoles of D and A, respectively. κ is the orientation factor defined as $\kappa \equiv \hat{\mu}_D \cdot \hat{\mu}_A - 3(\hat{\mu}_D \cdot \hat{\mathbf{R}}_{DA})(\hat{\mathbf{R}}_{DA} \cdot \hat{\mu}_A)$, which can range from –2 to 2. The circumflex symbol ^ denotes the unit vector associated with its corresponding vector, $\vec{\mu}_D$, $\vec{\mu}_A$ and $\vec{\mathbf{R}}_{DA}$, respectively. Figure 2.1 shows several relative $\hat{\mu}_D$-$\hat{\mu}_A$ orientations and the corresponding κ values. For a random distribution of dipole moments, $\kappa^2 = 2/3$. The neglect of higher order multipole interaction terms is justified except when the electronic transitions of D and A are only weakly allowed.

Förster showed that Eq. (1) can be expressed as [1, 29]

$$k_{ET} = \tau_f^{-1}(\overline{R}_0 / R)^6, \tag{2.3}$$

where τ_f is the empirical fluorescence lifetime of the non-interacting donor. $\overline{R}_0$ is the critical molecular separation defined by Förster [29] as

$$\overline{R}_0^6 = \frac{9000 \ln 10 \kappa^2 \eta_D^0}{128 \pi^6 n^4 N} \int_0^\infty f_D(\nu) \varepsilon_A(\nu) \frac{d\nu}{\nu^4}. \tag{2.4}$$

Here, η_D^0 is the quantum yield of the donor, n is the refractive index of the solvent, N is the Avogadro's number, ν is frequency in wavenumber, $f_D(\nu)$ is the spectral distribution of the donor fluorescence and $\varepsilon_A(\nu)$ is the molar decadic extinction coefficient of the acceptor. The integral in Eq. (2.4) defines the spectral overlap between the donor's fluorescence and the acceptor's absorption, which is equal to 1 for perfect overlap. When R equals $\overline{R}_0$, energy transfer time equals the fluorescence lifetime of D*. Based on experimental data, Duysens

$$\kappa \equiv \hat{\mu}_D \cdot \hat{\mu}_A - 3(\hat{\mu}_D \cdot \hat{R}_{DA})(\hat{R}_{DA} \cdot \hat{\mu}_A)$$

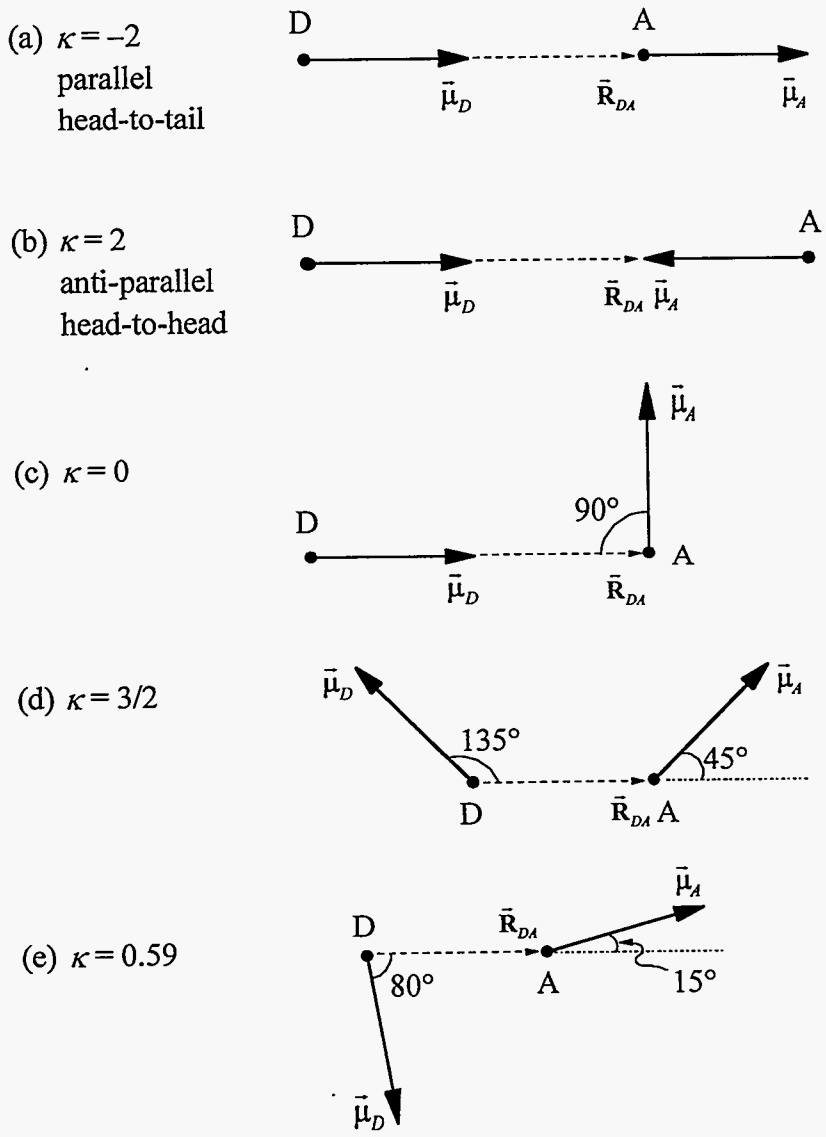

Figure 2.1 Examples of donor-acceptor arrangements and their corresponding orientation factors κ, which ranges from –2 to 2. The solid straight lines are the vectors of transition dipole moments ($\vec{\mu}_D$ and $\vec{\mu}_A$), while the dashed lines shows the vector ($\vec{R}_{DA}$) connecting the donors and the acceptors (marked by the solid circles at one end of $\vec{\mu}_D$ or $\vec{\mu}_A$ vectors). Here $\vec{\mu}_D$, $\vec{\mu}_A$ and $\vec{R}_{DA}$ are assumed to be in the same plane for illustration purpose, however, this assumption does not generally hold in real systems.

[32] reported that $\overline{R}_0 \sim 60$ Å for chlorophyll *a*, which is generally larger than the values (10 to 50 Å) for typical dye molecules in solution.

2.2.2 Implications and Validity of Assumptions Made in Conventional Förster Energy Transfer

Förster-type energy transfer for weakly coupled D and A molecules is expected to be dominant when the transitions involved are dipole-allowed. Due to the dipole-dipole nature of the coupling, the transfer rate is inversely proportional to the sixth power of the donor-acceptor distance *R*, Eq. (2.3). (Spin-flip energy transfer is not taken into account in Förster theory.) Fulfilling of the *co-linear* and the *resonance* conditions will optimize the transfer rate. The former condition is easily understood by examining Figure 2.1 and Eq. (2.4), which is proportional to κ^2. When the transition dipole moments of the donor and the acceptor are in line, either head-to-head or head-to-tail configuration, κ^2 is the largest with a value of 4. The meaning of *resonance* condition is demonstrated in Figure 2.2. The value of the spectral overlap integral, which defines the magnitude of overlap between donor fluorescence and acceptor absorption spectra, ranges from 0 to 1. The value of 1, which is the optimal value for Förster transfer, corresponds to perfect overlap. Since Förster theory assumes that the "hot" excited donor must undergo vibrational relaxation before energy transfer, the best spectral overlap will occur when the excitation energy transfers downhill from donor to acceptor, Figure 2.2 (a). That is, the energy transferred from D* to A is less than $h\nu$, the excitation energy of D. The difference in energy is lost in the thermalization process with the surrounding medium.

Long-distance energy transfer, however, has been observed in systems with forbidden transitions, either resulting from symmetry- or spin-forbiddenness. These transitions can become weakly allowed by mixing with proper molecular vibrations and with states having different multiplicities, respectively.

If the system has allowed-donor and forbidden-acceptor transitions, $\overline{R}_0$ will be small

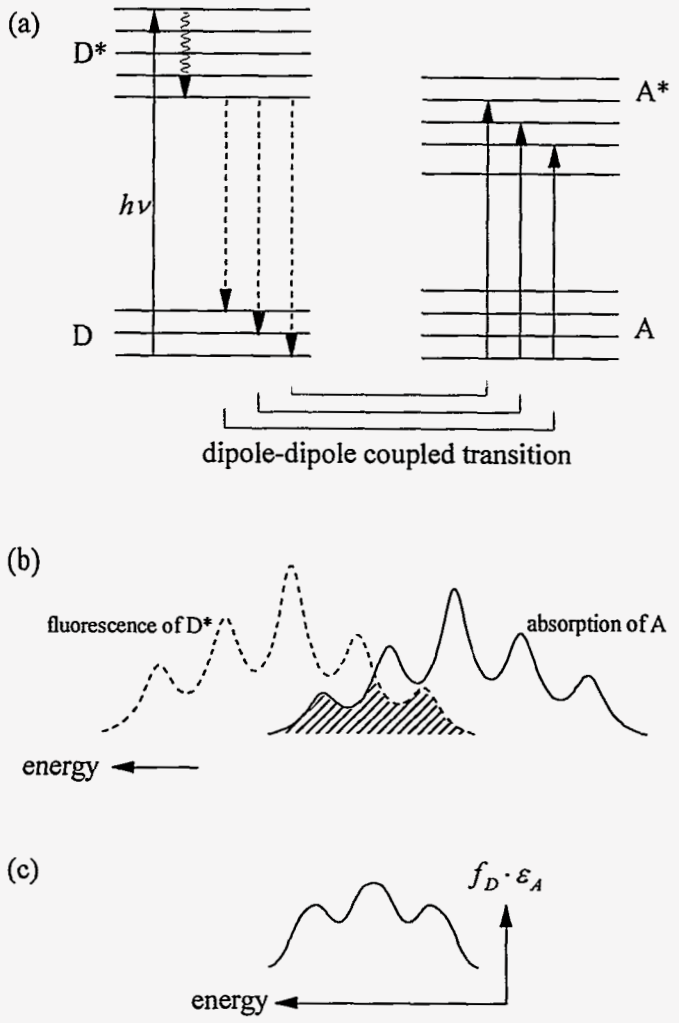

Figure 2.2 (a) A simplified energy level diagram showing the fulfillment of the *resonance* condition between the donor and acceptor. Following the excitation of energy $h\nu$, the donor molecule undergoes vibrational relaxation with the surrounding medium as shown by the wavy arrows. The energy is transferred to the acceptor which is in *resonance* with D* via the dipole-dipole coupling. For easy comparison, the ground states of D and A are offset to the same energy. (b) An illustration of the resonance condition by the spectral overlap (shaded area) between the donor's fluorescence (dashed line) and the acceptor's absorption (solid line). (c) A plot of the spectral overlap from (b). Due to the partial overlap as demonstrated in the figure, the value of the spectral overlap integral is between 0 and 1.

and energy transfer can be triggered by higher-order Coulombic coupling terms. As the donor-acceptor distance R decreases, the higher-order interactions plays more and more important role in the donor-acceptor coupling. As demonstrated by Dexter [3], to describe the energy transfer dynamics for this situation it is now necessary to include terms such as the dipole-quadrupole interaction which results in an inverse eighth power dependence on R. This type of energy transfer may be observed in systems which have dipole-forbidden transitions and R larger than the van der Waals radius (When the donor and the acceptor are within the van der Waals contact, energy transfer usually occurs via electron exchange, which is described in Section 2.3).

In Förster theory, after the donor is optically excited, vibrational relaxation, which takes place in ~ 1 ps, occurs prior to the transfer of energy to the acceptor. This assumption is not valid for energy transfer processes which occur on a sub-picosecond time scale. Again, Förster-Dexter theory is questionable for strongly coupled arrays of chromophores. As already mentioned, Förster theory is not applicable to systems in which the D and A optical transitions suffer from significant inhomogeneous broadening from structural heterogeneity. The structural heterogeneity leads to a distribution of D-A energy gap values which can result in dispersive (non-single exponential) kinetics for the D*→A energy transfer process, see the following subsection. For example, the inhomogeneous broadenings of the Q_y-absorption transitions of photosynthetic complexes are ~ 100-200 cm^{-1}. (For example, the B800 and B850 bands of LH2 from *Rps. acidophila* exhibit an inhomogeneous broadening of 120 cm^{-1} at 4.2 K [21].)

2.2.3 Kolaczkowski-Hayes-Small (KHS) Theory for Weak Coupling Energy Transfer

In 1994, Small and coworkers developed a theory (KHS) which takes into account dispersive kinetics of energy transfer [25]. They took into account both the inhomogeneous and homogeneous broadening of the optical transitions in order to properly describe the excitation transfer kinetics observed in photosynthetic protein complexes. The theory allows

for calculation of energy transfer rates without having to resort to experimental spectra for the spectral overlap factor of Förster theory which, in any event, is a questionable thing to do when the spectral bands are inhomogeneously broadened. What is required for calculations with KHS theory are experimental values of Franck-Condon factors for pigment intramolecular vibrations and protein phonons, the width of the distribution of D-A energy gap values and the homogeneous and inhomogeneous contributions to the widths of the relevant spectral transitions. The electronic coupling matrix element must be calculated. The theory is valid for finite temperature. KHS theory has been shown to be in good agreement with electron transfer rates in photosystem II [33], energy transfer in light-harvesting complexes 2 from bacteria [13, 26, 27]. For brevity, only key equations involved in the derivation are included in this section. One can start by writing down the rate constant for adiabatic energy transfer as [34, 35]

$$k_{DA}(\Omega) = V^2 \int_{-\infty}^{\infty} e^{-i\Omega t} f(t)\, dt, \tag{2.5}$$

where Ω and V are the adiabatic electronic energy gap and the appropriate electronic coupling matrix element between the donor and the acceptor states. Note that circular frequency is chosen to be the energy unit here. The kernal $f(t)$ has the form of

$$f(t) = \int d\Omega\, G(\Omega) e^{i\Omega t}. \tag{2.6}$$

In Eq. (2.6), $G(\Omega)$ is the thermally averaged nuclear factor and its form depends on whether the phonon is localized or delocalized‡. By working within the Condon approximation and being guided by hole burning data, the appropriate form of $f(t)$ for delocalized phonons is

$$f(t) = \exp(-\tilde{S}) \exp\{S \exp(-\sigma^2 t^2/2)[(2\bar{n}+1)\cos(\omega_m t) + i \sin(\omega_m t)]\}, \tag{2.7}$$

---

‡ If the participation of high-frequency intramolecular vibrations is required due to a large donor-acceptor gap, the phonon contribution to the nuclear factor retains the form of Eq. (3) of Ref. [25] as for the delocalized phonons.

where $\bar{n} = [\exp(\hbar\omega_m / kT) - 1]^{-1}$ is the mean thermal occupation number for the phonons. In arriving at Eq. (2.7), a Gaussian function carrying a width of $\sim 2\sigma$ is used to approximate the one-phonon profile having a mean frequency of ω_m. S is the Huang-Rhys factor at 0 K which characterizes the electron-phonon coupling strength. In the mean phonon frequency approximation employed,

$$\tilde{S} = S \operatorname{ctnh}(\hbar\omega_m / 2kT). \tag{2.8}$$

The Franck-Condon factor for the zero-phonon process is in fact $\exp(-\tilde{S})$. $f(t)$ is further approximated by expanding Eq. (2.7) in terms of t and anything higher than quadratic terms is neglected. This approximation is valid for $(\omega_m t_{1/2})^2 < 1$ where $t_{1/2} = \omega_m^{-1}[2S(2\bar{n}+1)]^{1/2}$, and it is expected not to break down at temperatures much lower than ~ 50 K (see the argument presented in Ref. [25]). As discussed in Ref. [25], the zero-phonon process only plays a minor role in energy transfer for inhomogeneously broadened systems such as photosynthetic protein complexes. As a result, it will be of little consequence if the contribution from zero-phonon lines is deleted by introducing the multiplicative factor $[1 - \exp(-\tilde{S})]$ into $f(t)$. By taking the Fourier transform, the expression for energy transfer rate is obtained as

$$k_{DA}(\Omega, T) = 2\pi V^2 (1 - e^{-\tilde{S}})[(2\pi\tilde{S}(\sigma^2 + \omega_m^2))^{-1/2} e^{-(\Omega - S\omega_m)^2 / 2\tilde{S}(\sigma^2 + \omega_m^2)}] \tag{2.9}$$

where the electronic energy gap $\Omega = \omega_D - \omega_A > 0$.

Since the system considered is inhomogeneously broadened, it is necessary to average Eq. (2.9) with a proper distribution function f_Ω for Ω to address the problem of dispersive kinetics. If f_Ω adopts a Gaussian form, the averaged rate becomes

$$\langle k_{DA}(T) \rangle = 2\pi V^2 (1 - e^{-\tilde{S}})[2\pi(\Gamma^2 + \tilde{S}(\sigma^2 + \omega_m^2))]^{-1/2} e^{-(\Omega_0 - S\omega_m)^2 / 2[\Gamma^2 + \tilde{S}(\sigma^2 + \omega_m^2)]}. \tag{2.10}$$

Here Γ^2 is the variance for f_Ω. As pointed out in Refs. [25, 36], Γ^2 and $\tilde{S}(\sigma^2 + \omega_m^2)$ are, respectively, associated with inhomogeneous and homogeneous broadening. If the following condition

$$S(\sigma^2+\omega_m^2) >> \Gamma^2 \tag{2.11}$$

is satisfied, $\langle k_{DA}(T)\rangle \approx k_{DA}(\Omega=\Omega_0,T)$. That is, the energy transfer kinetics is non-dispersive.

Eq. (2.9) and (2.10) can be modified to account for the electronic dephasing by substituting, everywhere, $\tilde{S}(\sigma^2+\omega_m^2)$ by $\Sigma^2(T)\equiv(\tilde{\Gamma}/2)^2+\tilde{S}(\sigma^2+\omega_m^2)$. Here $\tilde{\Gamma}$ denotes the homogeneous broadening contribution from dephasing. Therefore, Eq. (2.10) is now

$$\langle k_{DA}(T)\rangle = 2\pi V^2(1-e^{-\bar{S}})[2\pi(\Gamma^2+\Sigma^2)]^{-1/2}e^{-(\Omega_0-S\omega_m)^2/2(\Gamma^2+\Sigma^2)}. \tag{2.12}$$

Analogous to Eq. (2.11), the criterion for non-dispersive kinetics becomes

$$\Sigma^2=(\tilde{\Gamma}/2)^2+\tilde{S}(\sigma^2+\omega_m^2) >> \Gamma^2. \tag{2.13}$$

There are experimental data indicating that high frequency Franck-Condon modes can play significant roles in energy transfer by fulfilling the necessary spectral overlap requirement of Förster theory [13, 26]. Eq. (2.12) of KHS theory may be modified to include the contributions from intramolecular vibrations by writing it as

$$\langle k_{DA}(T)\rangle = 2\pi V^2(1-e^{-\bar{S}})(2FC_{loc})[2\pi(\Gamma^2+\Sigma^2)]^{-1/2}e^{-(\Omega_0-\omega_{loc}-S\omega_m)^2/2(\Gamma^2+\Sigma^2)}, \tag{2.14}$$

where ω_{loc} and FC_{loc} are the frequency and Franck-Condon factor for the intra-molecular vibration modes involved in the energy transfer [13, 26].

2.3 Energy Transfer via Electron Exchange Interactions

When the donor-acceptor separation is small, there will be an appreciable charge distribution overlap. Multipole expansion in the interaction energy V, which is used to evaluate the matrix elements in the Fermi-Golden Rule expression, Eq. (2.1), is no longer a good approach. The matrix element part in Eq. (2.1) has to be replaced by

$$\left|\sum_{i,j}\langle D^*A|\frac{q_iq_j}{r_{ij}}|DA^*\rangle\right|^2, \tag{2.15}$$

where the summation is carried out over all pairs of charges on D and A. By substituting the antisymmetrized spin-orbital functions into expression (2.15) and simplifying using the Condon-Slater rules and assuming that the ground and excited states on the donor molecule differ by only one spin-orbital ($u_n \neq u'_n$), and similarly for the acceptor molecule ($v_n \neq v'_n$), one obtains

$$\begin{aligned}
&\sum_{i,j}\langle D^* A|\frac{q_i q_j}{r_{ij}}|DA^*\rangle \\
&=\sum_{i,j}\langle u_1u_2u_3\ldots u_n;v_1v_2v_3\ldots v_m|\frac{q_i q_j}{r_{ij}}|u_1u_2u_3\ldots u'_n;v_1v_2v_3\ldots v'_m\rangle \\
&=\langle\phi_n(1)\phi_m(2)|\frac{1}{r_{12}}|\phi'_n(1)\phi'_m(2)\rangle\langle\sigma_n(1)|\sigma'_n(1)\rangle\langle\sigma_m(2)|\sigma'_m(2)\rangle \\
&-\langle\phi_n(2)\phi_m(1)|\frac{1}{r_{12}}|\phi'_n(1)\phi'_m(2)\rangle\langle\sigma_m(1)|\sigma'_n(1)\rangle\langle\sigma_n(2)|\sigma'_m(2)\rangle
\end{aligned} \tag{2.16}$$

where each spin-orbital function u_k or v_k equals the product of a space function ϕ_k and a spin function σ_k (either as spin up α or spin down β). The numbers 1 and 2 are dummy indices denoting the positions of the two electrons. The two terms in Eq. (2.16) represent the matrix elements resulting from the *Coulombic* and the *exchange* couplings. The former reduces to Förster theory in the dipole-dipole coupling approximation. The conservation of spins on both donor and acceptor molecules in Förster energy transfer is clear by examining Eq. (2.16), since the Coulombic term will vanish unless $\sigma'_n = \sigma_n$ and $\sigma'_m = \sigma_m$. Nevertheless, for exchange coupling, both $\sigma'_m = \sigma_n$ and $\sigma'_n = \sigma_m$ have to be satisfied during the energy transfer. Thus, energy transfer by electron exchange can occur when the spins of the donor and the acceptor are interchanged simultaneously during the process. This provides the mechanism for the triplet-triplet energy transfer, such as the deactivation of excited triplet BChl *a* by triplet carotenoid molecules.

The distance (R) dependence of $\langle \phi_n(2)\phi_m(1)|1/r_{12}|\phi'_n(1)\phi'_m(2)\rangle$ is rather complicated, but generally speaking it dies off rapidly as R increases. Following Dexter [3], the energy transfer rate can be expressed as

$$k_{ET} = K \cdot J \cdot \exp(-2R/L). \tag{2.17}$$

Here K is a constant related to the specific interaction involved, J is the normalized spectral overlap between D and A and L is a constant of the order of the molecular size.

Figure 2.3 is a simple pictorial diagram showing the Dexter energy transfer via electron exchange, as well as the diagram for energy transfer via Coulombic interactions. As shown in Figure 2.3 (a), the exchange interaction induces the simultaneous jumps of electrons 1 from D* to A* and 2 from A to D, which is different from Figure 2.3 (b) for Coulombic coupling where electrons remain in the same molecules. Actually the electron exchange coupling is a pure quantum mechanical property which rises from the *indistinguishability* of electrons in the presence of appreciable wavefunction overlap. Unlike Förster energy transfer which is feasible with R as large as tens of angstrom, Dexter type can only occur when the donor and the acceptor are in close contact (usually $\lesssim$ 5 Å).

2.4 Molecular Excitons

2.4.1 Mott-Wannier and Frenkel Excitons

As mentioned in Section 2.1, the excitation is delocalized in the strong coupling limit and is often referred to as an *exciton*, which is a term now widely used in photosynthesis. The term *exciton*, which originally derives from solid state physics, is introduced to denote its quasi-particle nature — the wave-like properties of delocalization and the particle-like properties of effective mass, definite momentum and energy.

The *Mott-Wannier exciton*, which is commonly observed in covalent solids such as Ge, Si and CdS and ionic crystals with large dielectric constants (such as Cu_2O), is actually an electron-hole pair weakly bound by an attractive electrostatic force, see Figure 2.4 (a).

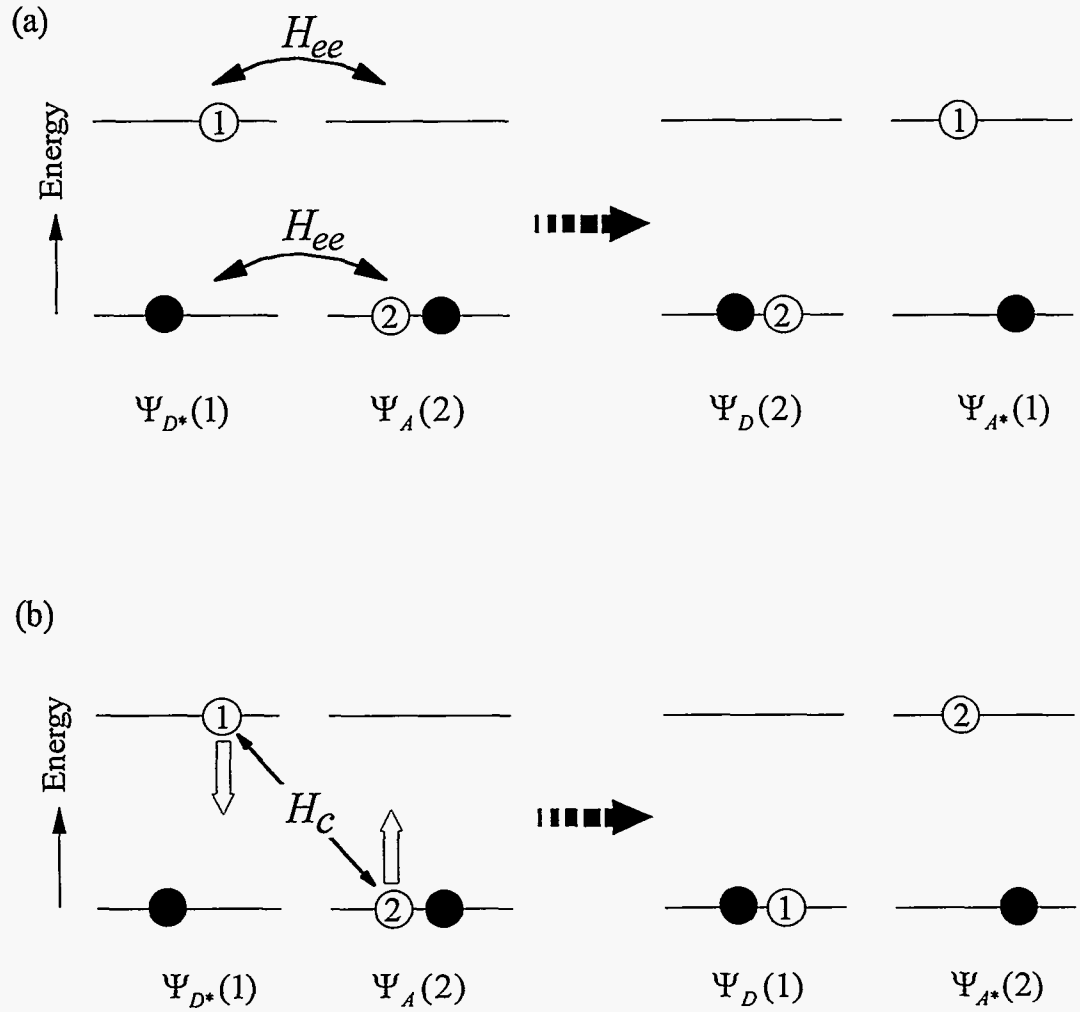

Figure 2.3 Schematic representation of excitation energy transfer via (a) electron exchange H_{ee} and (b) coulombic interactions H_c. The orbitals of the donor and the acceptor are depicted qualitatively by two-level systems with two electrons in each molecule. The *active* electrons are shown by open circles labeled as 1 and 2. The solid circles represent the *inactive* electrons whose interactions with others are nearly unaffected by the energy transfer processes. As shown in (a), exchange coupling induces simultaneous jumps of electrons 1 and 2 to the other molecules. In (b), the coulombic interaction makes electron 1 to return to the ground state and electron 2 is excited to the higher state.

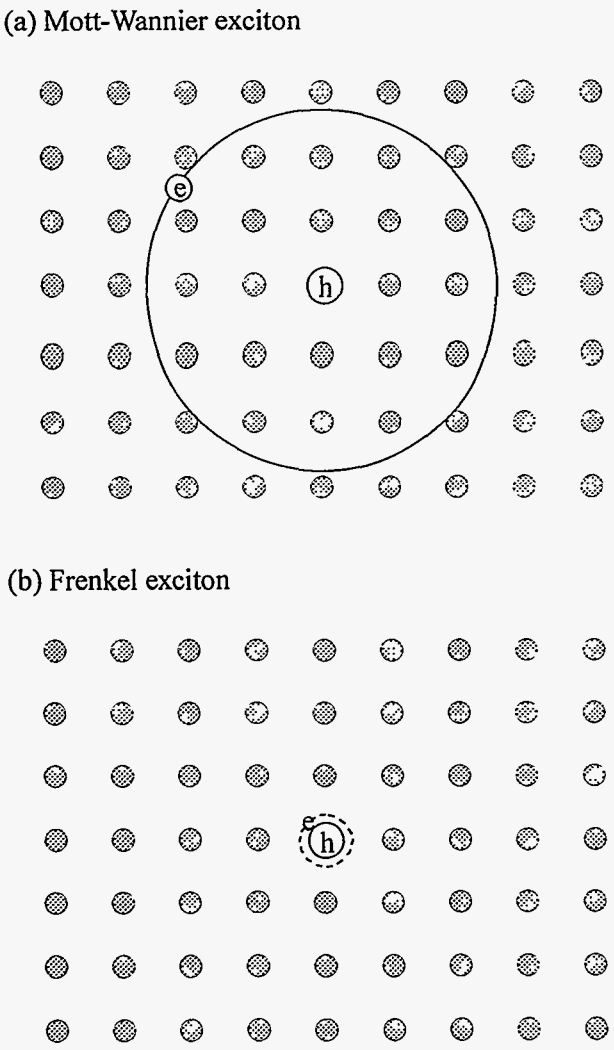

Figure 2.4 Conceptual illustration of Mott-Wannier exciton (a) and Frenkel exciton (b). The shaded circles shows the lattice molecules, while e and h label electrons and holes, respectively. In (a), the exciton is a bound electron-hole pair which moves as a unit in the crystal. The electron-hole separation is large relative to the lattice constant. In (b), it depicts a tightly bounding electron-hole pair confined within one molecule, which corresponds to an excited molecule. Due to the coupling with other molecules, this Frenkel exciton is not localized on one molecule. To correctly describe it quantum mechanically, it is necessary to use a superposition of wavefunctions of the entire lattice (i.e. in the Bloch wave form) due to the fact that there is equal probability for each molecule to be associated with the exciton.

The electron-hole separation is large compared with the lattice constant. Mott-Wannier excitons can propagate in the crystal to transport energy, but not electricity, due to the fact that they are charge-neutral. Readers interested in Mott-Wannier excitons may consult Refs. [4, 37-39] for further information.

Now consider the *tightly-bound* exciton which has the electron and the hole confined within one molecule. Actually, this essentially pictures an excited state of a single molecule, Figure 2.4 (b). Due to the coupling interactions between molecules in the crystal, the excitation energy will be passed from molecule to molecule like a wave instead of being localized on one site. This type of exciton is a collective electronic excitation of molecules, the *Frenkel exciton*, which has been thoroughly studied in molecular crystals such as naphthalene and anthracene. In a "perfect" crystal with no defects or phonons which undergo scattering with the exciton (meaning $T \rightarrow 0$ K), the Frenkel exciton is a perfectly delocalized state with a Bloch-type wavefunction. Every molecule in the crystal has an equal probability of being excited and for every level of the exciton band there is a definite phase relationship defined by the coefficients of the Bloch wavefunction. Thus, the concept of energy transfer loses its meaning. Of course, creation of a perfect Frenkel exciton in the laboratory is another matter, e.g. crystals have surfaces and there is no such thing as a perfect crystal. Nevertheless, exciton theory allows one to calculate band structures which can be used to calculate the group velocities (v_g) of exciton wavepackets with well-defined $\underline{\mathbf{k}}$, where $\underline{\mathbf{k}}$ is the wavevector. One can then define the exciton coherence length $l_{coh} = v_g/\gamma$, where γ is the scattering frequency (via defects or phonons) of the wavepacket. When $l_{coh} >>$ a unit cell length, the exciton is referred to as delocalized. When l_{coh} is comparable to a unit cell length it is referred to as localized and energy transfer can then be treated as an incoherent hopping process [40, 41].

In recent years the term exciton has been widely used by workers interested in the nature of the excited electronic states of photosynthetic antenna complexes such as the cyclic

C_n LH2 and LH1 complexes of purple bacteria. With reference to earlier discussion of these complexes, it is clear that one is dealing with nano-excitons and, therefore, that the concepts of wavepacket velocity and coherence length are quite ill-defined. All that is implied by a "perfect" exciton of LH1 or LH2 is that it is completely delocalized with each BChl *a* molecules of the ring having an equal probability of being excited. The problem becomes more interesting when one realizes that proteins are glass-like, meaning that they are nothing like perfect crystals. Thus, the effects of energy disorder (diagonal or off-diagonal) become very important as discussed in Chapters 5 and 6. In the case of diagonal energy disorder, the exciton levels become localized in the limit of very strong disorder which is defined by the disorder-induced couplings between the zero-order exciton levels being much larger than the zero-order splittings between the exciton levels. As shown in Chapter 6, the B850 and B875 rings of LH2 and LH1, respectively, fall in the category of weak disorder, meaning that the exciton levels are neither perfectly localized or delocalized.

The following two subsections, 2.4.2 and 2.4.3 are a review of the Frenkel exciton theory in the static lattice approximation, meaning that exciton-phonon coupling is neglected as well as the effects of energy disorder.

2.4.2 An Excitonically Coupled Dimer — A Simple Example

Consider an isolated molecule with the eigenfunction φ^i and the eigenenergies E^i defined by the Hamiltonian H

$$H\varphi^i = E^i\varphi^i, \tag{2.18}$$

where $i = g$ or e denote the ground and excited states. Now introduce one more identical molecule into the system which couples with the other via the intermolecular potential energy V. The total wavefunction and energy for the system with both molecules in the ground state may be written as

$$\psi^g = \varphi_1^g\varphi_2^g \tag{2.19a}$$

$$\left\langle \psi^g \left| H_1 + H_2 + V \right| \psi^g \right\rangle = 2E^g + D^g, \tag{2.19b}$$

where the subscripts 1 and 2 denote the two molecules and $D^g \equiv \left\langle \psi^g \left| V \right| \psi^g \right\rangle$. The presence of the term D^g is the so-called *van der Waals interaction* or *dispersion energy* for the ground state.

The wavefunctions for the electronically excited dimer may be written as

$$\Psi(\pm) = 2^{-1/2}(\psi_1^e \pm \psi_2^e), \tag{2.20}$$

The coefficient $2^{-1/2}$ holds with the neglect of overlap between the two monomers. ψ_1^e and ψ_2^e are the wavefunctions describing excitation localized on molecules 1 and 2, respectively. That is,

$$\psi_1^e = \varphi_1^e \varphi_2^g \tag{2.21a}$$

$$\psi_2^e = \varphi_1^g \varphi_2^e. \tag{2.21b}$$

Eq. (2.20) gives the delocalized basis set (wavefunctions) for the excited dimer, while Eq. (2.21a-b) defines the localized states. The energy of the excited dimer is given by

$$\left\langle \Psi(\pm) \left| H_1 + H_2 + V \right| \Psi(\pm) \right\rangle = E^g + E^e + D^e \pm M, \tag{2.22}$$

where D^e and V are defined as followed

$$D^e \equiv \left\langle \psi_1^e \left| V \right| \psi_1^e \right\rangle = \left\langle \psi_2^e \left| V \right| \psi_2^e \right\rangle \tag{2.23a}$$

$$M \equiv \left\langle \psi_1^e \left| V \right| \psi_2^e \right\rangle = \left\langle \psi_2^e \left| V \right| \psi_1^e \right\rangle. \tag{2.23b}$$

Similar to D^g, D^e is the van der Waals interaction or dispersion energy but for the excited dimer. M, the *resonance transfer integral*, determines the resonance energy transfer time and the *dimer (exciton) splitting*. The relative orientation of the two molecules determines the sign of M. Figure 2.5 shows several examples of M with different monomer orientations in the dipole-dipole approximation. $(D^e - D^g)$ is the so-called *solvent shift* in the excitation energy between the isolated and coupled monomers. Usually, molecules in the excited state interact more strongly than in the ground state. As a result, the solvent shift causes a decrease in the excitation energy. See Figure 2.6 for an illustration of D^g, D^e and M. As

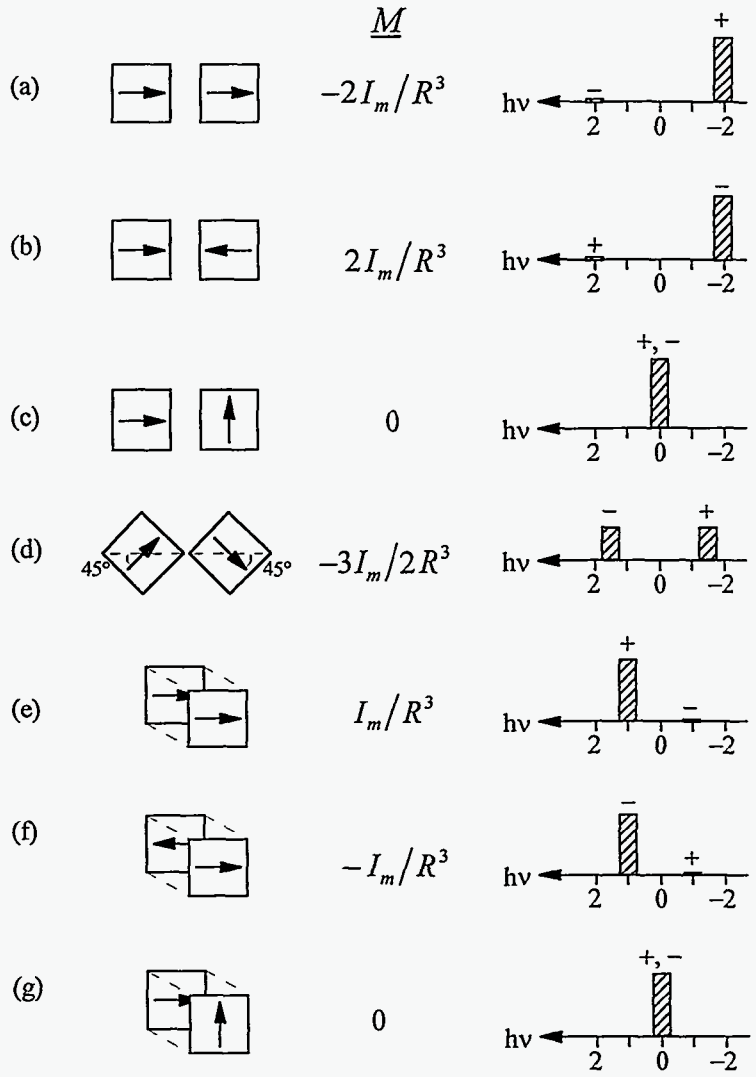

Figure 2.5 Schematic representations of seven dimer arrangements with their dimer splittings M, Eq. (2.23b), and their redistribution of oscillator strength. Although the squares and the associated arrows are meant to show the BChl (Chl) molecular planes and their Q_y transition dipole moments, they are applicable to other molecules with in-plane transition dipoles. Geometries (a) through (d) are co-planar, while (e) through (g) are stacked. The dimer splittings are calculated within the dipole-dipole approximation (Eq. (2.2)), i.e. $M = \kappa I_m/R^3$ where $I_m = |\vec{\mu}_1||\vec{\mu}_2| = |\vec{\mu}_1|^2 = |\vec{\mu}_2|^2$ is the transition dipole strength of the monomer. The right-most column qualitatively shows the spectra of the dimer with the energy ($h\nu$) in units of I_m/R^3 and the excitation energy of a monomer is defined as zero. + and – signs are used to label the wavefunctions $\Psi(+)$ and $\Psi(-)$. See text for further explanation.

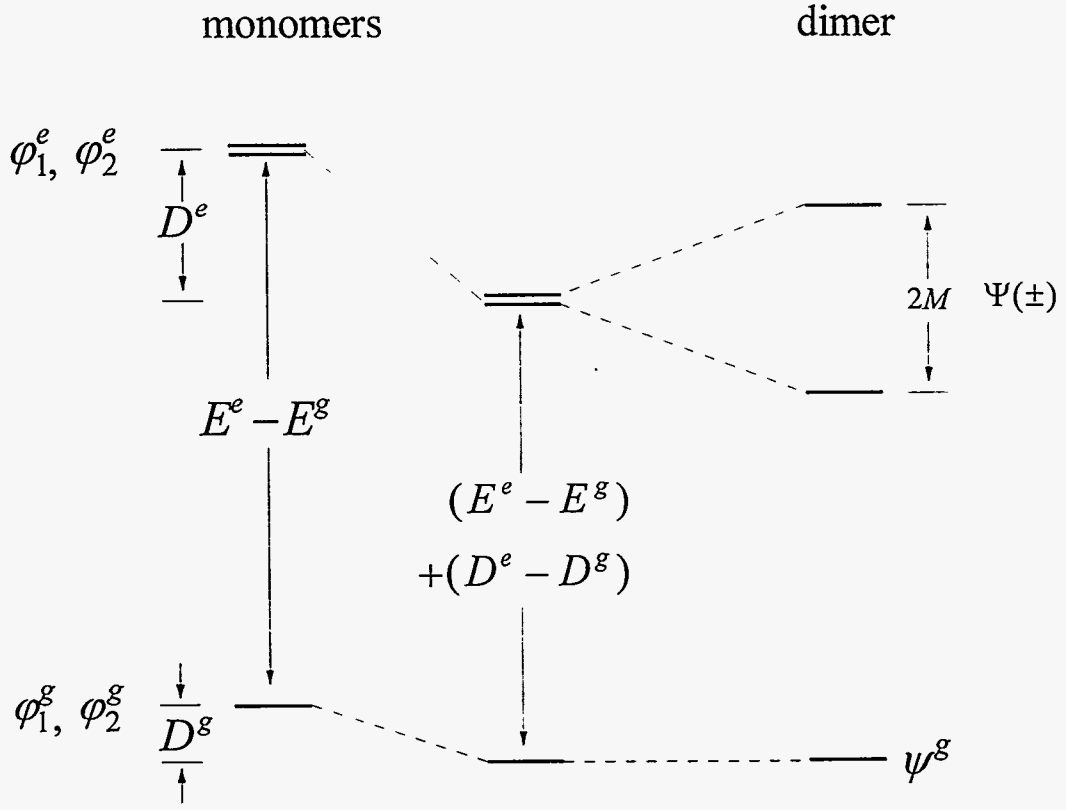

Figure 2.6 Energy level diagram of two isolated monomers and an excitonically coupled dimer. φ_i^g and φ_i^e ($i = 1, 2$) are the ground and the excited state wavefunctions for monomer i, respectively. For the dimer, ψ^g is the wavefunction for the ground state, while $\Psi(\pm)$ are the dimer (exciton) wavefunctions. The dispersion interaction between monomers introduced a decrease of $D^e - D^g$ in excitation energy, which is often referred to as the solvent shift. The exciton levels are further split by an energy of $2M$. The geometric arrangement of the two monomers determines which of the exciton wavefunctions $\Psi(\pm)$ will have higher energy, see Figure 2.5, as well as the magnitude and the sign of M. See text for further explanation.

indicated in Eq. (2.22), Figures 2.5 and 2.6, $\Psi(+)$ and $\Psi(-)$ are not degenerate, but are separated by a splitting of $2M$. The splitting of excited states is an important characteristic of excitonic behavior. In addition to this splitting, the formation of exciton is often accompanied with a redistribution of oscillator strength, which is described below.

The transition dipole strength of the dimer $I_d(\pm)$ from ψ^g to $\Psi(\pm)$ can be expressed in terms of I_m, the transition dipole strength of the isolated molecules

$$I_d(\pm) = \left| \left\langle \psi^g \left| \underline{\mu}_1 + \underline{\mu}_2 \right| \Psi(\pm) \right\rangle \right|^2 = I_m(1 \pm \cos\theta), \tag{2.24}$$

where θ is the angle between the transition dipole moments of the two monomers. $\underline{\mu}_1$ and $\underline{\mu}_2$ are the dipole moment operators for the two molecules. The right-most column of Figure 2.5 shows how $I_d(\pm)$, the transition dipole strength, varies with the angle θ.

In Figure 2.5(a), the head-to-tail arrangement having a κ value of -2 gives a negative M equal to $-2I_m / R^3$. According to Eq. (2.22), $\Psi(+)$ and $\Psi(-)$ are the lower and upper dimer states, respectively. Since $\theta = 0°$, I_d is $2I_m$ for $\Psi(+)$ and 0 for $\Psi(-)$, see Eq. (2.24). That is, the upper dimer component is transition forbidden. Similarly, one can generate the qualitative pictures as shown in Figure 2.5(b) through (g). Note that cases (a) and (b) are indistinguishable from a spectral point of view (only the lower dimer state is transition allowed). In (a) the lower dimer state is $\Psi(+)$, while in (b) it is $\Psi(-)$. In contrast to (a) and (b), where the transition dipoles lie in the same plane, (e) and (f) of the stacked configurations illustrate the situation where only the upper dimer components are transition allowed. In Figure 2.5(d), the two split dimer components are transition allowed and both carry a transition dipole strength equal to I_m. The dimer arrangements shown in Figure 2.5(c) and (g) have M values of zero and do not result in splitting or a redistribution of the transition dipole strength.

When the dimer states, $\Psi(+)$ and $\Psi(-)$, are spectrally well-resolved one can excite either of them selectively to initially create delocalized dimer states. The excitation energy

undergoes coherent oscillation between the two monomers with a frequency of M, with M in the unit of circular frequency. Strictly speaking, this oscillation does not represent energy transfer since it does not alter the initially excited level. For real energy transfer to occur, the excitation ultimately needs to be localized on one of the two monomers. Such localization could result from self-trapping due to exciton-phonon coupling or energy disorder when the dimer is imbedded in a bath. It is possible to initially create a state with excitation localized on one of the two monomers if the frequency width of the excitation pulse is wider than $2M$.

2.4.3 Extension from the Dimer to Molecular Crystals and Circular Aggregates

The aforementioned exciton for a Frenkel-like dimer can be easily extended to cover molecular aggregates and crystals. For a system containing n molecules, the wavefunction for the excitation energy localized on molecule α located at position $\underline{\alpha}$ is

$$\psi_{\alpha}^{e} = \varphi_{\alpha}^{e} \prod_{\alpha=0(\beta\neq\alpha)}^{n-1} \varphi_{\beta}, \tag{2.25}$$

where φ_{β} is the ground state wavefunction for molecule β and φ_{α}^{e} is the excited state wavefunction for molecule α. Eq. (2.25) is analogous to Eq. (2.21). Let H_{α} be the energy operator for the α-th molecule and $V_{\alpha\beta}$be the interaction between molecules α and β. The Hamiltonian for the exciton states is

$$H = \sum_{\alpha} H_{\alpha} + \sum_{\alpha,\beta}{}' V_{\alpha\beta}. \tag{2.26}$$

A general solution to Eq. (2.26) is

$$\Psi(\underline{\mathbf{k}}) = n^{-1/2} \sum_{\alpha} \exp(i\underline{\mathbf{k}}\cdot\underline{\alpha})\, \psi_{\alpha}^{e}. \tag{2.27}$$

$\underline{\mathbf{k}}$ is the wavevector and is determined from the boundary conditions. Eq. (2.27) is of Bloch-wave form and is only true for the system with one molecule per unit cell. (Consult Ref. [5] for the analogous exciton wavefunction of Eq. (2.27) for crystals with more than one translationally inequivalent molecule per unit cell.) For a 3-dimensional crystal with only one molecule per unit cell,

$$\underline{\mathbf{k}} = \sum_{p=1}^{3} \frac{2\pi}{N_p} q_p \underline{\mathbf{b}}_p , \tag{2.28}$$

where $\underline{\mathbf{b}}_p$ (p = 1, 2 and 3) are the reciprocal lattice vectors defined according to the direct lattice vectors $\underline{\mathbf{a}}_{p'}$ as $\underline{\mathbf{b}}_p \cdot \underline{\mathbf{a}}_{p'} = \delta_{pp'}$. q_p is an integer confined within the range $-N_p/2 \le q_p \le N_p/2$. N_p satisfies the relation $n \equiv N_1 N_2 N_3$ when the crystal is assumed to be parallelepiped. For more details, see Ref. [5]. The delocalized basis set in the form of Eq. (2.27) for a cyclically coupled array, which is relevant to the light-harvesting complexes of purple bacteria, is given in the Appendix, Eq. (A.3). The Hamiltonian for a linear aggregate has been diagonalized and the expression for the exciton wavefunctions can be found in Refs. [42, 43].

As in the case of dimer, the degeneracy of the excited energy levels will be lifted to produce an exciton band. However, the band will span a range of $\sim 4M$ for molecular crystals or circular aggregates (in the nearest neighbor approximation) instead of $2M$ as shown earlier for dimers.

2.4.4 Exciton-Phonon Coupling

So far in the discussion of excitons, it has been assumed that the molecules are fixed rigidly at the lattice points. In this section, the consequences of the molecular displacements from equilibrium positions in connection to excitons are discussed. This formulation was outlined for excitons in molecular crystals by Davydov [5].

To proceed, the Hamiltonian of the exciton is conveniently written in terms of the localized basis representation as

$$H_{ex}(\underline{\mathbf{R}}) = \sum_n [\varepsilon + \sum_m{}' D_{nm}(\underline{\mathbf{R}})] B_n^+ B_n + \sum_{n,m}{}' M_{nm}(\underline{\mathbf{R}}) B_m^+ B_n , \tag{2.29}$$

where ε is the free-molecule excitation energy for the transition of interest and B_n and B_n^+ are the annihilation and creation operators for the nth site, respectively. D_{nm} and M_{nm} are, respectively, the dispersion and resonance-energy transfer matrix elements between sites n and m. The term containing the summation of D_{nm}, which corresponds to D^e in Eq. (2.23a)

for a dimer, is the total interaction of the excited molecule with all of the ground-state molecules. The term M_{nm} governs the excitation energy transfer from molecule n to m. Similar to M of Eq. (2.23b), M_{nm} results in delocalization of the excitation energy and the exciton band. The presence of the D_{nm} and M_{nm} terms introduces the dependence on the lattice configuration $\underline{\mathbf{R}}$ into the Hamiltonian $H_{ex}(\underline{\mathbf{R}})$. Eq. (2.29) may be expanded in a Taylor series about $\underline{\mathbf{R}} = 0$, the equilibrium position, and all the terms higher than the linear term are discarded. Therefore, it becomes

$$H_{ex}(\underline{\mathbf{R}}) = H_{ex}(0) + H_{ex-ph}^{(1)} + H_{ex-ph}^{(2)}, \tag{2.30}$$

where

$$H_{ex}(0) = \sum_{n}[\varepsilon + \sum_{m}{}' D_{nm}(0)]B_n^+ B_n + \sum_{n,m}{}' M_{nm}(0)B_m^+ B_n \tag{2.31}$$

is the Hamiltonian for the non-deformed lattice which yield the crude adiabatic energies for the exciton levels. $H_{ex-ph}^{(1)}$ and $H_{ex-ph}^{(2)}$ are linear exciton-phonon coupling terms given by

$$H_{ex-ph}^{(1)} = \sum_{n,m}{}' B_n^+ B_m \sum_{j=1}^{6}[R_n^j(\frac{\partial M_{nm}}{\partial R_n^j})_0 + R_m^j(\frac{\partial M_{nm}}{\partial R_m^j})_0] \tag{2.32a}$$

$$H_{ex-ph}^{(2)} = \sum_{n,m}{}' B_n^+ B_n \sum_{j=1}^{6}[R_n^j(\frac{\partial D_{nm}}{\partial R_n^j})_0 + R_m^j(\frac{\partial D_{nm}}{\partial R_m^j})_0]. \tag{2.32b}$$

In these two equations, $j = 1, 2, 3, \ldots, 6$ denote the six (three translational and three rotational) degrees of freedom of the molecule. To see the physics behind $H_{ex-ph}^{(1)}$ and $H_{ex-ph}^{(2)}$ better, it is more convenient to express them in terms of the creation and annihilation operators $b_{s,\underline{\mathbf{q}}}^+$ and $b_{s,\underline{\mathbf{q}}}$ for an sth branch phonon of wavevector $\underline{\mathbf{q}}$ and the delocalized basis set operators $B^+(\underline{\mathbf{k}})$ and $B(\underline{\mathbf{k}})$. The Hamiltonian for the phonons in the absence of excitons is

$$H_{ph}^0 = \sum_{s,\underline{\mathbf{q}}} \hbar\omega_s(\underline{\mathbf{q}})(b_{s,\underline{\mathbf{q}}}^+ b_{s,\underline{\mathbf{q}}} + 1/2). \tag{2.33}$$

$B^+(\underline{\mathbf{k}})$ and $B(\underline{\mathbf{k}})$ are in the delocalized representation which diagonalize $H_{ex}(0)$ and are related to B_n by

$$B_n = N^{-1/2}\sum_{\underline{\mathbf{k}}} B(\underline{\mathbf{k}})\exp(i\underline{\mathbf{k}}\cdot\underline{\mathbf{n}}). \tag{2.34}$$

Now $H^{(1)}_{ex-ph}$ and $H^{(2)}_{ex-ph}$ become

$$H^{(1)}_{ex-ph} = N^{-1/2}\sum_{\underline{\mathbf{k}},\underline{\mathbf{q}},s} F_s(\underline{\mathbf{k}},\underline{\mathbf{q}})\, B^{+}(\underline{\mathbf{k}}+\underline{\mathbf{q}})\, B(\underline{\mathbf{k}})(b_{s,\underline{\mathbf{q}}}+b^{+}_{s,-\underline{\mathbf{q}}}) \tag{2.35a}$$

$$H^{(2)}_{ex-ph} = N^{-1/2}\sum_{\underline{\mathbf{k}},\underline{\mathbf{q}},s} \chi_s(\underline{\mathbf{q}})\, B^{+}(\underline{\mathbf{k}})\, B(\underline{\mathbf{k}})(b_{s,\underline{\mathbf{q}}}+b^{+}_{s,-\underline{\mathbf{q}}}). \tag{2.35b}$$

$F_s(\underline{\mathbf{k}},\underline{\mathbf{q}})$ and $\chi_s(\underline{\mathbf{q}})$ characterize the exciton-phonon coupling strength which are given by

$$F_s(\underline{\mathbf{k}},\underline{\mathbf{q}}) = \sum_{j,m(\neq 0)} e^j_s(\underline{\mathbf{q}})\beta^j_s(\underline{\mathbf{q}})\left[\left(\frac{\partial M_{0m}}{\partial R^j_0}\right)_0 + e^{i\underline{\mathbf{q}}\cdot\underline{\mathbf{m}}}\left(\frac{\partial M_{0m}}{\partial R^j_m}\right)_0\right]e^{i\underline{\mathbf{k}}\cdot\underline{\mathbf{m}}} \tag{2.36a}$$

$$\chi_s(\underline{\mathbf{q}}) = \sum_{j,m(\neq 0)} e^j_s(\underline{\mathbf{q}})\beta^j_s(\underline{\mathbf{q}})\left[\left(\frac{\partial D_{0m}}{\partial R^j_0}\right)_0 + e^{i\underline{\mathbf{q}}\cdot\underline{\mathbf{m}}}\left(\frac{\partial D_{0m}}{\partial R^j_m}\right)_0\right], \tag{2.36b}$$

respectively. $e^j_s(\underline{\mathbf{q}})$ is the jth component of a unit polarization vector for the sth phonon branch with wavevector $\underline{\mathbf{q}}$, while $\beta^j_s(\underline{\mathbf{q}})$ is the *rms* amplitude of the corresponding motion [5, 44]. For more details regarding the derivation, see Refs. [5, 45-47].

The connecting bridges of Eqs. (2.35a-b) in the delocalized basis set and Eqs. (2.32a-b) in the localized basis set are the unitary-transformation-related Eq. (2.34) and

$$B(\underline{\mathbf{k}}) = N^{-1/2}\sum_{n} B_n \exp(-i\underline{\mathbf{k}}\cdot\underline{\mathbf{n}}). \tag{2.37}$$

Section IV.A.4 of Ref. [47] provides a nice discussion relating the choice between delocalized and localized representations.

Let us proceed to examine the physical meanings behind $H^{(1)}_{ex-ph}$ and $H^{(2)}_{ex-ph}$. The former relates to the inter-site coupling terms M. When the lattice vibrates about its equilibrium positions, the interactions between molecules change accordingly. F_s in fact characterizes the coupling strength between the phonon modes and the inter-site interactions. $H^{(1)}_{ex-ph}$ is the term responsible for the elastic and inelastic scattering of the excitons from one $\underline{\mathbf{k}}$ value to another. During the process, the total number of excitons remains the same while that of phonons changes. The simple diagrams in Figure 2.7 depict this scattering process.

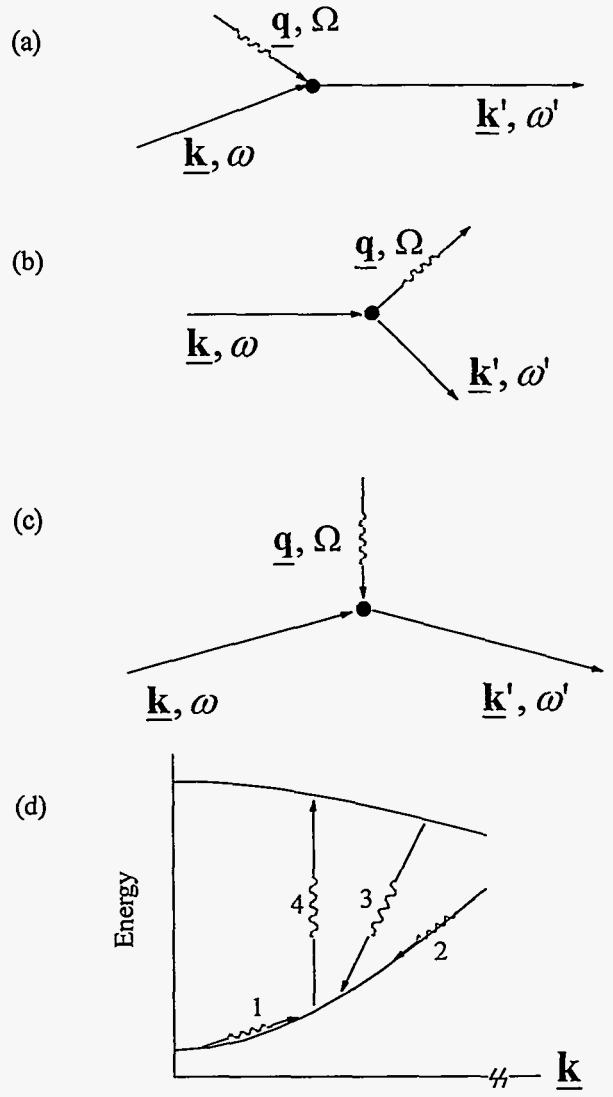

Figure 2.7 Vector diagrams (a-c) and a dispersion curve (d) showing examples of exciton-phonon scattering events (a-c). The exciton (solid arrows) having the wavevector $\underline{k}$ and the frequency ω is scattered to an exciton state of $\underline{k}'$ and ω'. The phonon (wavy arrows) absorbed or emitted in the process has a wavevector of $\vec{q}$ and a frequency of Ω. Both the energy and the momentum conservation must be fulfilled in the scattering events. Processes (a), (c), 1 and 4 show phonon-absorption processes, while (b), 2 and 3 are for phonon-emission. Intra- and inter-exciton band scattering processes are depicted in 1-2 and 3-4, respectively. For crystals with more than one molecule per unit cell, inter-exciton band scattering may occur with no change in $\underline{k}$ (governed by the coupling term Eq. (2.36b)), such as the process 4 in (d).

The term $H^{(2)}_{ex-ph}$. is diagonal in the delocalized representation and it is associated with the dispersion term D. The lattice vibration results in a fluctuation of the center of gravity of the exciton bands. χ_S characterizes how strong the change in exciton energy is with respect to the phonons. $H^{(2)}_{ex-ph}$ will shift the equilibrium configuration of the intermolecular coordinates to a new position, i.e. it causes a lattice deformation over the region the exciton excitation is distributed. If the lattice deformation is very large, the exciton will become localized. The name *polaron*† is introduced to refer to the exciton plus its accompanying lattice deformation under the influence of $H^{(2)}_{ex-ph}$.

Since $H^{(1)}_{ex-ph}$ and $H^{(2)}_{ex-ph}$ arises from different properties of the molecular crystals, their relative magnitude varies from system to system and depends on the electronic excitation of the same sample.

2.4.5 Inter-Exciton Level Relaxation Processes — Beyond the Condon Approximation

When the excitonic level splittings associated with the chromophores are large relative to the dephasing of the levels (i.e. in the strong coupling limit), the Condon approximation, which assumes that the electronic coupling is independent of the phonon coordinates, is no longer valid. In this strong coupling regime, the excitonic wavefunctions are determined by the Hamiltonian which already includes the static intermolecular potential energy. This is the potential that into Fermi-Golden rule expression of the Förster theory, see Section 2.2.1. The spectral density is a Franck-Condon factor weighted density of the final states of the energy transfer process. For strongly excitonically coupled systems such as the B850 molecules of LH2 and the B875 molecules of LH1, relaxation between exciton levels is induced by phonons which modulate the intermolecular pigment-pigment interactions. We refer to those phonons as promoting modes with coordinates Q_p (frequency ω_p). With V_{int} the interchromophore interaction, $(\partial V_{\text{int}} / \partial Q_p)_0 Q_p$ is the term that enters the Fermi-Golden rule

---

† The term polaron also often refers to an electron plus its lattice deformation in solid state physics.

when linear coupling in the phonon coordinate Q_p is assumed. One obtains for the downward inter-exciton level relaxation rate:

$$\frac{2\pi}{\hbar}\left|\left\langle \Psi^f \left|\left(\frac{\partial V_{\text{int}}}{\partial Q_p}\right)_0\right|\Psi^i\right\rangle\left\langle n_p+1\left|Q_p\right|n_p\right\rangle\right|^2 \rho(\Omega), \tag{2.38}$$

where Ψ^i and Ψ^f are the wavefunctions of the initial and final exciton levels, and Ω is the energy gap between the two levels. The phonon coordinate of the promoting mode can be expressed in terms of the creation and annihilation operators b^+ and b:

$$Q_p = (\hbar/2\omega_p)^{1/2}(b_p + b_p^+). \tag{2.39}$$

Thus, Eq. (2.38) becomes

$$\frac{\pi}{\omega_p}(\bar{n}_p+1)\left|\left\langle \Psi^f \left|\left(\frac{\partial V_{\text{int}}}{\partial Q_p}\right)_0\right|\Psi^i\right\rangle\right|^2 \rho(\Omega-\omega_p), \tag{2.40}$$

where the argument of the spectral density ρ indicates that the effective energy gap has been reduced by one quantum of the promoting mode. $\rho(\Omega-\omega_p)$ is still a weighted density of states involving other phonons which are Franck-Condon active. Note that promoting modes need not be Franck-Condon active. In Eq. (2.40), $\bar{n}_p$ is the thermal occupation number, $[\exp(\hbar\omega_p/kT)-1]^{-1}$. In the high temperature limit, $(\bar{n}_p+1) \propto T$.

A more detailed treatment [5, 47] reveals that the electronic matrix element in Eq. (2.40) describes how the resonance energy transfer matrix elements associated with the excitonically coupled chromophores vary with Q_p.

2.5 References

[1] Förster, Th. *Ann. Physik* **1948**, *2*, 55.

[2] Struve, W. S. In *Anoxygenic Photosynthetic Bacteria*: Blankenship, R. E.; Madigan, M. T.; Bauer, C. E. Eds.; Kluwer: Dordrecht, 1995; Chapter 15.

[3] Dexter, D. L. *J. Chem. Phys.* **1953**, *21*, 836.

[4] Knox, R. S. *Theory of Excitons*, Academic Press: New York, 1963.

[5] Davydov, A. S. *Theory of Molecular Excitons*; Plenum Press: New York, 1971.

[6] Pearlstein, R. M. In *Photosynthesis,* Vol. 1; Govindjee Ed.; Academic Press: New York, 1982; Chapter 7.

[7] van der Laan, H.; Schmidt, Th.; Visschers, R. W.; Visscher, K. J; van Grondelle, R.; Völker, S. *Chem. Phys. Letts.* **1990**, *170*, 231.

[8] Shreve, A. P.; Trauman, J. K.; Frank, H. A.; Owens, T. G.; Albrecht, A. C. *Biochim. Biophys. Acta.* **1991**, *973*, 93.

[9] Reddy, N. R. S.; Small, G. J.; Seibert, M.; Picorel, R. *Chem. Phys. Letts.* **1991**, *181*, 391.

[10] Reddy, N. R. S.; Small, G. J. *J. Chem. Phys.* **1991**, *94*, 7545.

[11] Reddy, N. R. S.; Cogdell, R. J.; Zhao, L. Small, G. J. *Photochem. Photobiol.* **1993**, *57*, 35.

[12] Monshouwer, R.; de Zarate, I. O.; van Mourik, F.; van Grondelle, R. *Chem. Phys. Lett.* **1995**, *246*, 341.

[13] Chapter 3; Wu, H.-M.; Savikhin, S.; Reddy, N. R. S.; Jankowiak, R.; Cogdell, R. J.; Struve, W. S.; Small, G. J. *J. Phys. Chem.* **1996**, *100*, 12022.

[14] Koepke, J.; Hu, X.; Muenke, C.; Schulten, K. Michel, H. *Structure*, **1996**, 4, 581.

[15] Sauer, K.; Cogdell, R. J.; Prince, S. M.; Freer, A. A.; Isaacs, N. W.; Scheer, H. *Photochem. Photobiol.*, **1996**, *64*, 564.

[16] Sietermann, D. *Biochim. Biophys. Acta* **1985**, *811*, 325.

[17] Cogdell, R. J.; Frank, H. A. *Biochim. Biophys. Acta* **1987**, *895*, 63.

[18] Shreve, A. P.; Trautman, J. K.; Frank, H. A.; Owens, T. G.; Albrecht, A. C. *Biochim. Biophys. Acta* **1991**, *1058*, 280.

[19] Frank, H. A.; Farhoosh, R.; Aldema, M. L.; DeCoster, B.; Christensen, R. L.; Gebhard, R.; Lugtenburg, J. *Photochem. Photobiol.* **1993**, *57*, 49.

[20] Hu, X.; Ritz, T.; Damjanovic, A.; Schulten, K. *J. Phys. Chem. B* **1997**, *101*, 3854.

[21] Wu, H.-M.; Reddy, N. R. S.; Small. G. J. *J. Phys. Chem. B* **1997**, 101, 651.

[22] Reddy, N. R. S.; Picorel, R.; Small, G. J. *J. Phys. Chem.* **1992**, *96*, 6458.

[23] Wu, H.-M.; Reddy, N. R. S.; Cogdell, R. J.; Muenke, C.; Michel, H.; Small, G. J. *Mol. Cryst. Liq. Cryst.* **1996**, *291*, 163.

[24] Chapter 4; Wu, H.-M.; Ratsep, M.; Jankowiak, R.; Cogdell, R. J.; Small, G. J. *J. Phys. Chem. B* **1997**, *101*, 7641.

[25] Kolaczkowski, S. V.; Hayes, J. M.; Small, G. J. *J. Phys. Chem.* **1994**, *98*, 13418.

[26] Reddy, N. R. S.; Wu, H.-M.; Jankowiak, R.; Picorel, R.; Cogdell, R. J.; Small, G. J. *Photosynth. Res.* **1996**, *48*, 277.

[27] van der Laan, H.; De Caro, C.; Schmidt, Th.; Visschers, R. W.; van Grondelle, R.; Fowler, G. J. S.; Hunter, C. N.; Völker, S. *Chem. Phys. Letts.* **1993**, *212*, 569.

[28] Fowler, G. J. S.; Hess, S.; Pullerits, T.; Sundström, V.; Hunter, C. N. *Biochem.* **1997**, *36*, 11282.

[29] Förster, Th. *Discuss. Faraday Soc.* **1959**, *27*, 7.

[30] Atkins, P. W. *Molecular Quantum Mechanics*, 2nd Ed., Oxford: London, 1983, p.198.

[31] Hirschfelder, J. O.; Meath, W. J. *Adv. Chem. Phys.* **1967**, *12*, 3.

[32] Duysens, L. N. M. *Prog. Biophys.* **1964**, *14*, 48.

[33] Chang, H.-C.; Jankowiak, R.; Reddy, N. R. S.; Small, G. J. *Chem. Phys.* **1995**, *197*, 307.

[34] Kubo, R.; Toyozawa, Y. *Prog. Theor. Phys.* **1955**, *13*, 160.

[35] Englman, R. *Nonradiative Decay of Ions and Molecules in Solids*; North-Holland: Amsterdam, 1979.

[36] Small, G. J.; Hayes, J. M.; Silbey, R. J. *J. Phys. Chem.* **1992**, *96*, 7499.

[37] Dresselhaus, G. *Phys. Chem. Solids* **1956**, *1*, 14.

[38] Elliott, R. J. *Phys. Rev.* **1957**, *108*, 1384.

[39] Sturge, M. D. In *Excitons*, Rashba, E. I.; Sturge, M. D. Eds., North-Holland Publishing: Amsterdam, 1982, p.5.

[40] Silbey, R. *Annu. Rev. Phys. Chem.* **1976**, *27*, 203.

[41] Knox, R. S. *Top. Photosynth.* **1977**, *2*, 55.

[42] Hochstrasser, R. M.; Whiteman, J. D. *J. Chem. Phys.* **1972**, *56*, 5945.

[43] Fidder, H.; Knoester, J.; Wiersma, D. A. *J. Chem. Phys.* **1991**, *95*, 7880.

[44] Craig, D. P.; Dissado, L. A. *Chem. Phys.* **1976**, *14*, 89.

[45] Venkataraman, G.; Sahni *Rev. Mod. Phys.* **1970**, *42*, 409.

[46] Burland, D. M.; Zewail, A. H. *Adv. Chem. Phys.* **1979**, *40*, 369.

[47] Johnson, C. K.; Small, G. J. In *Excited States*: Lim, E. C. Ed.; Academic Press: New York, 1982; Vol. 6, p.97.

CHAPTER 8. CONCLUSIONS

The results presented in this dissertation establish that non-photochemical hole burning spectroscopy combined with pressure and external electronic (Stark) fields is an powerful approach for the study of the Q_y-excited state electronic structures and energy transfer/relaxation dynamics of photosynthesis antenna complexes.

The high pressure data for the isolated LH2 complex or chromatophores from *Rps. acidophila* establish that the B800 → B850 energy transfer rate is resilient to significant pressure-induced changes in the B800-B850 energy gap, consistent with data reported earlier for the LH2 complex of *Rb. sphaeroides*. In addition, the energy transfer rate is also weakly dependent on temperature and mutation. All told, the B800-B850 energy gap can be varied between 450 and 1050 cm^{-1} without affecting the ~1 picosecond rate by more than a factor of 3. It was shown that the conventional Förster theory (which assumes the absence of inhomogeneous broadening of the Q_y-transition) based on spectral overlap between the B800 fluorescence origin band and the B850 absorption band is incorrect. The results of our theoretical calculations indicate that the Förster-like B800 → B850 transfer rate involves spectral overlap with weakly allowed BChl *a* modes which build on B850 which, with low frequency protein phonons, provide a quasi-continuum of final states. It is to be emphasized that the calculations involved no adjustable parameters.

Zero-phonon action spectroscopy was used to determine and characterize the lowest energy exciton level (B870) of the B850 ring of LH2 and of the B875 ring (B896) of the LH1 complex. (The results for B896 are not included in this dissertation.) Based on the structure for LH2, it was argued that the exciton level structure of the B850 ring of *Rps. acidophila* cannot be understood without taking into account energy disorder. A new theory based on symmetry-adapted basis defect patterns (BDP) was developed to provide for deeper insight and ease of computation in the study of the effects of disorder (diagonal or off-diagonal) on

cyclic arrays of coupled chlorophylls. The theory was used to explain the 200 cm^{-1} displacements of B870 below the B850 band maximum and B870's absorption intensity which is 3-5% of the total absorption intensity of the B850 ring. (The results are for *Rps. acidophila*.) It was found that in the absence of energy disorder, the average displacement of B870 is ~ 150 cm^{-1} at 4.2 K. The low temperature B850 absorption profile established that the B850 ring is in the weak energy disorder limit.

The BDP-based disorder calculations utilized a value of –320 cm^{-1} for the nearest dimer-dimer coupling, which differs by ~ 120 cm^{-1} from the value (–200 cm^{-1}) calculated using the room temperature X-ray structure of *Rps. acidophila*. The larger value of –320 cm^{-1} for the low temperature calculations was mandated by the T-dependence of the B850 absorption band which reveals that LH2 (isolated or in chromatophores) undergoes a quite subtle and non-denaturing structural change near 150 K. (This is also the case for the LH1 complex.) Theoretical analysis of the thermal broadening of the B850 band led to the conclusion that the nearest neighbor BChl *a* dimer-dimer coupling is about 40% larger for the low temperature structure. Comparison of the T-dependencies of the B850 band of *Rps. acidophila* and *Rb. sphaeroides* (LH2 structure unknown) indicates that the above coupling for the latter is about 20% weaker than for the former at all temperatures. It was suggested that the α, β-polypeptide pairs may be more loosely packed in *Rb. sphaeroides*. This is consistent with the pressure-dependent data obtained for the two LH2 complexes. It is interesting that the temperature dependencies for the B850 band of *Rps. acidophila* and *Rs. molischianum* are very similar since their LH2 complexes are, respectively, 9-mers and 8-mers of α, β-polypeptide pairs and there is only marginal sequence homology between the pairs of the two species. When the structure of the LH2 complex of *Rb. sphaeroides* becomes available, the suggestion that the α, β-pairs are more loosely packed in *Rb. sphaeroides*, which leads to a weakening in nearest neighbor BChl *a*-BChl *a* couplings, can be tested.

New data on the pressure dependencies of the B800 and B850 bands of LH2 and the B875 band of LH1 were reported for several species. In addition, the linear pressure shift rates for the B870 level of the B850 ring and B896 level of the B875 ring were determined. A theoretical model was introduced in order to understand why the linear pressure shifts for the B850 and B875 bands and the B870 and B896 exciton levels are ~ 4 to 6 times larger than the ~ −0.1 cm^{-1}/MPa shift rate of B800, which falls in the range of values observed for isolated chromophores in amorphous solids. The results of calculations with the model indicate that electron-exchange coupling, rather than electrostatic (Coulombic) coupling, between nearest BChl *a* neighbors of the B850 and B875 rings is primarily responsible for their unusually large pressure shifts. This assertion can be tested by electronic structure calculations since reasonable compressibility values are available.

Stark hole burning spectroscopy of bacterial and green algae antenna complexes was reported for the first time. The Stark data yield the dipole moment changes, $f \cdot \Delta\mu$, associated with the optical transitions from the ground electronic to excited Q_y-states. The dipole moment changes of B800 and B870 of LH2, B896 of LH1 and B825 of the FMO complex (*Cb. tepidum*) were determined. The values obtained fall in the range of ~0.5-1.2 D. Several conclusions were drawn. For the sake of brevity I mention only that: one cannot understand the Stark effect of the B850 and B875 rings without taking into account exciton localization effects produced by energy disorder and, therefore, the $f \cdot \Delta\mu$ values determined for B850 and B875 using classical Stark modulation spectroscopy are unreliable; the angle between $\Delta\underline{\mu}$ and the Q_y-transition dipole of BChl *a* in proteins is $\lesssim 15°$; and the protein-induced contribution to $\Delta\underline{\mu}$ is significant.

Understanding the excitation energy and electron transfer processes of photosynthetic complexes is a fascinating, challenging and important problem. A firm understanding of the processes is unattainable without a good understanding of the Chl Q_y-states. The candidate believes that her research has shown that the combination of spectral hole burning with

pressure and Stark fields are important new approaches for yielding data of very considerable importance to quantum chemists working on the excited state electronic structures of photosynthetic complexes.

APPENDIX

SYMMETRY ADAPTED BASIS DEFECT PATTERNS FOR ANALYSIS OF THE EFFECTS OF ENERGY DISORDER ON CYCLIC ARRAYS OF COUPLED CHROMOPHORES

A.1 Cyclic Arrays of Coupled Chromophores

Consider a molecule α in a cyclic (C_n) ring of n (≥ 3) identical chromophores undergoing an electronic transition to the state Ψ_α'. The *localized* wavefunction is given as

$$|\alpha\rangle = \Psi_\alpha' \prod_{\alpha=0(\beta\neq\alpha)}^{n-1} \Psi_\beta, \tag{A.1}$$

where Ψ_β is the ground state wavefunction for molecule β. If the interaction energy ($V_{\alpha\beta}$) between sites α and β is non-zero, the Hamiltonian for this cyclically coupled array in the absence of disorder is

$$H_0 = e\sum_{\alpha}^{n-1}|\alpha\rangle\langle\alpha| + \sum_{\alpha,\beta=0}^{n-1}{}' V_{\alpha\beta}|\alpha\rangle\langle\beta|, \tag{A.2}$$

where e is the excitation energy of the chromophore. The eigenfunctions of H_0 are wave-like and the excitation will no longer be localized at molecule α. The cyclic symmetry determines the delocalized wavefunctions to be [1]

$$|j\rangle = n^{-1/2}\sum_{\alpha} B^{j\alpha^*}|\alpha\rangle, \tag{A.3}$$

where $B = \exp(i2\pi/n)$. The factor of $n^{-1/2}$ holds when neglecting the overlap between chromophores. The quantum number j = 0, 1, …, (n-1) labels the 1-dimensional irreducible representations (reps) of the C_n group. Except for j = 0 and n/2 (n is even), each $|j\rangle$ has one degenerate partner, and together they give E-type reps. For example, when n = 9, the correspondence between quantum number j and group theoretical designation is j = 0 (A), j = {1, 8} (E_1), j = {2, 7} (E_2), j = {3, 6} (E_3) and j = {4, 5} (E_4). Or using another set of quantum numbers, the equivalent correspondence becomes j = 0 (A), j = {1, −1} (E_1), j = {2, −2} (E_2), j = {3, −3} (E_3) and j = {4, −4} (E_4). When n is even, there are two non-degenerate reps A (j = 0) and B (j = n/2).

In the nearest neighbor coupling approximation, the exciton energies are

$$E_j = e + 2V\cos(2\pi j/n), \tag{A.4}$$

where V is the nearest neighbor coupling energy.

In the presence of disorder, the total Hamiltonian becomes

$$H = H_0 + H_\lambda + H_\mathrm{v}, \tag{A.5}$$

where H_λ and H_v govern the diagonal and off-diagonal energy disorder, respectively, and are given as

$$H_\lambda = \sum_\alpha \lambda_\alpha |\alpha\rangle\langle\alpha| \tag{A.6}$$

$$H_\mathrm{v} = \sum_\alpha \mathrm{v}_\alpha (|\alpha\rangle\langle\alpha+1| + |\alpha+1\rangle\langle\alpha|). \tag{A.7}$$

To investigate how these two defect Hamiltonians couple with the zero-order delocalization levels it is convenient to express both in terms of the delocalized wavefunctions using

$$|\alpha\rangle = n^{-1/2} \sum_j B^{j\alpha} |j\rangle. \tag{A.8}$$

Eq. (A.6) becomes

$$H_\lambda = n^{-1} \sum_\alpha \sum_j \sum_k \lambda_\alpha B^{\alpha j} B^{\alpha k *} |j\rangle\langle k|. \tag{A.9}$$

Thus, for H_λ the coupling between delocalized exciton levels r and s, *i.e.* the element in the row r and column s of the Hamiltonian matrix, is

$$\langle r|H_\lambda|s\rangle = n^{-1} \sum_\alpha \sum_j \sum_k \lambda_\alpha B^{\alpha j} B^{\alpha k *} \delta_{rj} \delta_{ks} = n^{-1} \sum_\alpha \lambda_\alpha B^{\alpha (r-s)} \tag{A.10}$$

Similarly, for H_v we obtain

$$H_\mathrm{v} = n^{-1} \sum_\alpha \sum_j \sum_k \mathrm{v}_\alpha (B^{j\alpha} B^{k(\alpha+1)*} + B^{j(\alpha+1)} B^{k\alpha *}) |j\rangle\langle k|, \tag{A.11}$$

$$\langle r|H_\mathrm{v}|s\rangle = n^{-1} \sum_\alpha \mathrm{v}_\alpha B^{(r-s)\alpha} (B^{-s} + B^{r}). \tag{A.12}$$

A.2 Symmetry-Adapted Basis Defect Patterns (BDP)

With Eqs. (A.10) and (A.12), the Hamiltonian matrix can be constructed to calculate exciton level energies and oscillator strengths once the defect pattern λ_α and/or v_α at each chromophore α is determined. To systematically investigate the effects of energy disorder, symmetry adapted basis defect patterns (BDP) are introduced. The BDP transform like the irreducible representations of a C_n group. BDP may seem to have limited applications to real physical systems which exhibit random, rather than correlated, energy disorder. However, the usefulness of BDP will become apparent once one recognizes that any arbitrary defect pattern can be expressed as a superposition of the complete and orthogonal set of BDP, *vide infra*. Thus, one can examine the effects of each BDP on the ring exciton structure to determine which, if any, are of primary importance.

The procedure of generating the complete and orthogonal set of BDP for a C_n group is quite straightforward for those who are familiar with using projection operator technique to obtain π molecular orbitals of benzene or similar cyclic molecules [1, 2]. For brevity, the equations shown in the following are mainly for diagonal energy disorder. The corresponding equations for off-diagonal disorder can be obtained in a similar manner.

A.2.1 BDP for Diagonal Energy Disorder and Their Associated Selection Rules

The diagonal energy disorder at site α can be expressed as

$$\lambda_\alpha(e_{j,\pm}) = N_{j,\pm}\left[\cos\left(\frac{2\pi j\alpha}{n}\right) \pm \cos\left(\frac{2\pi j(\alpha-1)}{n}\right)\right], \tag{A.13}$$

for *e*-type patterns. (To avoid confusing BDP with exciton levels, lower case is used to indicate the symmetry of BDP.) The + and – signs denote the orthogonal partners of each degenerate pattern. $N_{j,\pm}$ is the normalization factor and is given as

$$N_{j,\pm}^{-2} = \sum_\alpha \left[\cos\left(\frac{2\pi j\alpha}{n}\right) \pm \cos\left(\frac{2\pi j(\alpha-1)}{n}\right)\right]^2. \tag{A.14}$$

Now one can define normalized basis defect vectors

$$\boldsymbol{D}_{j,\pm} = N_{j,\pm}(d^{\pm}_{j,0}, d^{\pm}_{j,1}, \ldots, d^{\pm}_{j,n-1}), \tag{A.15}$$

where the *d*-elements are given by the square-bracketed terms in Eq. (A.13). Figure 3 of Chapter 5 shows the normalized diagonal $e_{1,\pm}$ and $e_{2,\pm}$ BDP. The complete normalized coefficients of BDP for C_9 and C_8 groups are listed in Tables 1 and 2 of Chapter 6. Incorporation of the BDP into Eq. (A.10) leads to

$$\langle r|H_{\lambda}^{e_{j,\pm}}|s\rangle = \frac{\lambda_{j,\pm}N_{j,\pm}}{n}\sum_{\alpha}\left[\cos(\frac{2\pi j\alpha}{n}) \pm \cos(\frac{2\pi j(\alpha-1)}{n})\right]e^{i2\pi\alpha(r-s)/n}, \tag{A.16}$$

for $e_{j,\pm}$ BDP.

Before continuing to show the corresponding expressions for off-diagonal energy disorder, it is worthwhile to discuss first the *selection rule* associated with Eq. (A.16). For the diagonal elements of the coupling Hamiltonian, *i.e.* when $r = s$, we have

$$\begin{aligned}\langle r|H_{\lambda}^{e_{j,\pm}}|r\rangle &\propto \sum_{\alpha}\left[\left(B^{j\alpha} + B^{j\alpha^*}\right) \pm \left(B^{j(\alpha-1)} + B^{j(\alpha-1)^*}\right)\right] \\ &= \left(\frac{1-B^{jn}}{1-B^{j}} + \frac{1-B^{jn^*}}{1-B^{j^*}}\right) \pm \left[B^{-j}\left(\frac{1-B^{jn}}{1-B^{j}}\right) + B^{-j^*}\left(\frac{1-B^{jn^*}}{1-B^{j^*}}\right)\right]\end{aligned} \tag{A.17}$$

for any j. Since $B^{jn} = 1$, Eq. (A.17) equals zero. Furthermore, the off-diagonal elements are

$$\begin{aligned}\langle r|H_{\lambda}^{e_{j,\pm}}|s\rangle &\propto \sum_{\alpha}\left[\left(B^{j\alpha} + B^{j\alpha^*}\right) \pm \left(B^{j(\alpha-1)} + B^{j(\alpha-1)^*}\right)\right]B^{\alpha(r-s)} \\ &\propto \left(\frac{1-B^{(j+r-s)n}}{1-B^{j+r-s}} + \frac{1-B^{(j-r+s)n^*}}{1-B^{(j-r+s)^*}}\right) \\ &\pm \left[B^{-j}\left(\frac{1-B^{(j+r-s)n}}{1-B^{j+r-s}}\right) + B^{-j^*}\left(\frac{1-B^{(j-r+s)n^*}}{1-B^{(j-r+s)^*}}\right)\right]\end{aligned} \tag{A.18}$$

Again, $B^{[j\pm(r-s)]n} = 0$, since j, r and s are all integers. Care needs to be taken, however, when

$$r - s = \pm j, \tag{A.19}$$

which gives us the selection rule associates with Eq. (A.16). When $r - s = j$, the denominators of the second and the fourth terms of Eq. (A.18) are zero, though the

numerators of all four terms vanish. If $r-s=-j$, the first and the third terms have denominators of zero. That means in the presence of $e_{j,\pm}$ BDP exciton levels r and s will couple with each other if the condition $r-s=\pm j$ is met. It is not difficult to show that the above selection rule also applies to the non-degenerate a and b BDP which have non-vanishing coupling elements when

$$r-s=0 \tag{A.20}$$

and

$$r-s=\pm\frac{n}{2}, \tag{A.21}$$

respectively.

A.2.2 The Decomposition of Arbitrary Defect Patterns

Returning to Eq. (A.15), we define a non-singular matrix $\underline{\mathbf{D}}$ whose columns are the transposes of the row vectors defined by Eq. (A.15) plus the normalized BDP column vector associated with the a rep (n odd) or a and b reps (n even). If $\underline{\lambda}=(\lambda_0, \lambda_1,\ldots,\lambda_{n-1})$ is an arbitrarily chosen diagonal energy disorder pattern then

$$\underline{\mathbf{C}}^{\mathrm{T}}=\underline{\mathbf{D}}^{-1}\underline{\lambda}^{\mathrm{T}} \tag{A.22}$$

where $\underline{\mathbf{C}}=(C_0,C_1,\ldots,C_{n-1})$. The components of $\underline{\mathbf{C}}$ are the coefficients of the BDP basis vectors in the superposition that yield $\underline{\lambda}$. The beauty of Eq. (A.22) is that an arbitrary defect pattern can be decomposed into the superposition of BDP, which enables us to systematically investigate the effects of different BDP on the exciton level structure and spectrosopic properties of a C_n ring.

A.2.3 BDP for Off-Diagonal Energy Disorder and Their Associated Selection Rules

Following a procedure similar to that used in deriving Eq. (A.16), one obtains the corresponding expression for off-diagonal energy disorder

$$\langle r|H_{\mathrm{v}}^{e_{j,\pm}}|s\rangle=\frac{\mathrm{v}_{j,\pm}N_{j,\pm}}{n}\sum_{\alpha}\left[\cos(\frac{2\pi j\alpha}{n})\pm\cos(\frac{2\pi j(\alpha-1)}{n})\right]\times B^{\alpha(r-s)}(B^{-s}+B^{r}). \tag{A.23}$$

To visualize off-diagonal BDP on a cyclic ring, one can rotate the coefficients for diagonal BDP as shown in Figure 3 of Chapter 5 about the C_n axis by π/n to make them "bond-centered".

The aforementioned decomposition procedure, Eq. (A.22), also applies to patterns involving off-diagonal disorder or patterns involving both diagonal and off-diagonal disorder. The selection rule for diagonal energy disorder, Eq. (A.19), holds for off-diagonal disorder too, once one recognizes that the additional factor $(B^{-s} + B^{r})$ in Eq. (A.23) is independent of site number α and Eq. (A.23) can be simplified to Eq. (A.18). There is one exception, however, when applying the selection rule to b-type off-diagonal disorder. The factor $(B^{-s} + B^{r})$ will be zero when $r = 0$ and $s = n/2$, or *vice versa* (recall the selection rule for b BDP is $r - s = \pm n/2$, Eq. (A.21)). Therefore, the selection rules for b-type off-diagonal disorder are

$$r - s = \pm\frac{n}{2},\ r \neq 0 \text{ and } s \neq 0 \qquad \text{(A.24)}$$

A.2.4 Removal of Exciton Level Degeneracies as Predicted by Group Theory

Before ending this section, it is worthwhile to comment on the removal of exciton level degeneracies by BDP as predicted by group theory. The first order splitting of a degenerate exciton level r is determined by BDP of symmetry contained in the symmetric direct product $(E_r \times E_r)_+$. For a C_9 ring and r = 1-4 the symmetries of the BDP able to remove the degeneracies are e_2, e_4, e_3 and e_1, respectively. While for a C_8 ring and r = 1-3, those are e_2, b and e_2, respectively. However, a second-order mechanism for removal of degeneracy exists because of the off-diagonal coupling defined by Eqs. (A.16) and (A.23), as well as the associated selection rule, Eq. (A.19).

A.3 Application of BDP to Antenna Complexes of Purple Bacteria

Symmetry-adapted Basis defect patterns have been applied successfully to investigate spectroscopic properties of LH2 of C_8 and C_9 symmetry and LH1 of C_{16} from purple bacteria. Examples of using BDP to study the re-distribution of oscillator strengths and exciton level splitting can be found in Ref. [3] and Chapter 5 of this dissertation. The simulation of the B850 absorption band using $e_{1,-}$ and $e_{4,+}$ BDP [3] agreed well with experimental data. Another successful application is the simulation of the lowest exciton level, A, of B850 molecules using $e_{1,+}$ BDP with a half-Gaussian distribution for the disorder parameter λ_0(see Chapter 5). An important conclusion from these BDP studies is that of all BDP e_1 is the essential and necessary component in endowing the very weakly allowed A level with more intensity and while concurrently increasing the gap between A and E_1 levels. This effect is referred to as *hidden correlation* in Chapter 6. Our studies on random defects by expressing them as superpositions of BDP further suppose this point of view. The domination of e_1-type BDP over others gives us confidence for employing BDP to study spectroscopic properties with the convenience of fast and easy computation without losing the essential physics of the systems. More recently, as stimulated by our Stark hole burning results, the localization effects on exciton levels caused by BDP and random defect patterns was examined (see Chapter 6). Comparisons of effects of diagonal, off-diagonal, single-site and random defects on a C_n ring were discussed in Chapter 6.

A.4 REFERENCES

[1] Hochstrasser, R. M. *Molecular Aspects of Symmetry*, W. A. Benjamin, Inc: New York, 1966.

[2] Cotton, F. A. *Chemical Applications of Group Theory*, John Wiley & Sons, Inc., New York, 1971.

[3] Wu, H.-M.; Small, G. J. *Chem. Phys.* **1997**, 218, 225.